공학박사학위논문

Electric current density effect on recrystallization kinetic of ultra low carbon steel

저탄소강의 재결정 속도에 전류가 미치는 영향

2020년 **2**월

서울대학교 대학원

재료공학부

박주원

ABSTRACT

Electrically-assisted manufacturing (EAM) is a processing technique which controls the mechanical properties and microstructure of metals by applying electric current. EAM has been divided into two researches. One is electroplasticity, which controls the properties by applying pulsed electric current during deformation. Many researchers have reported that the applied electric current during deformation drastically affects the material properties such as yield stress, flow stress and elongation. The other is electropulsing treatment (EPT), which controls microstructural change of a conductive metallic materials without deformation. EPT is an effective technique that changes the microstructure of a metallic material and improves its physical properties by applying high electric current density. Through the understanding of electric current-assisted phenomenon, effect of electric current on recrystallization kinetic was evaluated based on the kinetic analysis.

First, the effect of electric current on recrystallization kinetics in interstitial free (IF) steel was investigated based on Vickers hardness measurements and microstructural observation. Electropulsing treatment (EPT) and furnace heat treatment (HT) for these work-hardened metals were carried out under various temperature and time conditions. The Vickers hardness value after EPT was clearly lower than that after HT at the same annealing condition. The microstructural

observation confirms that the reduced hardness value was resulted from recrystallization. This implies that the recrystallization kinetics was accelerated by the athermal effect distinct from Joule heating. To identify the athermal effect of the electric current on the recrystallization kinetics, the Johnson-Mehl-Avrami-Kolmogorov (JMAK) equation was adopted. The value of the Avrami exponent, which depends on the nucleation rate in recrystallization, was higher in EPT than in HT. In addition, it was observed that the activation energy for recrystallization was reduced in EPT compared to HT.

Secondly, one pulse experiments were conducted to determine the effect of current density on athermal effect. A single EPT is utilized and various electric current densities are considered with appropriate duration times to achieve the target peak annealing temperatures. The experimental results show that the degree of recrystallization tends to decrease with increasing the electric current density and then increase above a certain current density, which formed V-shaped grape when the peak annealing temperatures are 760 and 800℃. The athermal effect is examined by comparing the recrystallization fractions measured in HT with those obtained in the EPT. Moreover, we quantitatively calculate the increase of the recrystallization fraction resulted from the athermal effect using a newly modified Johnson-Mehl-Avrami-Kolmogorov (JMAK) equation adopting the additivity rule, and confirm that the athermal effect becomes prominent as the current density increases. We elucidate the athermal effect of the EPT annealing with dependence on the current density by introducing reduction of recrystallization activation

energy and effective temperature.

Lastly, in order to apply the previously quantified effective temperature to the electroplasticity, tensile behavior is analyzed by FE constitutive calculation. The parameters of the hardening equation that are well matched to the high temperature tension are derived. The tensile behavior of pulsed tension is predicted using the temperature history under electroplasticity. When the effective temperature was inserted into the grain boundary, the calculated stress-strain curve come to in good agreement with the experimental one. This proves that the athermal effect can be explained by introduction of the effective temperature even in electroplasticity.

From this research, fundamental understandings of the ahtermal effect of electric current were established. Through the kinetic analysis on the recrystallization of low carbon steel, it is clearly demonstrated that electric current accelerates the diffusion of atoms. Moreover, how much electric current density affects the athermal effect is quantified. This study provides an important index to electrically-assisted manufacturing.

Keywords: low carbon steel, interstitial free steel, extra deep drawing grade steel, electrically-assisted manufacturing (EAM), electroplasticity, recrystallization, kinetic analysis, Vickers hardness, electron backscatter diffraction (EBSD), athermal effect, effective temperature, constitutive equation, finite element calculation

Student number: 2014-21447

Contents

Chapter 2

Recrystallization kinetic changes with applying electric current on low carbon steel

Chapter 3

Effect of electric current density on recrystallization kinetic

LIST OF TABLES

LIST OF FIGURES

Chapter 1

Introduction

1.1 Electrically-assisted manufacturing (EAM)

Electrically-assisted manufacturing (EAM) is a processing technique which controls the mechanical properties and microstructure of metals by applying electric current. Researches concerning EAM have been divided into two main parts. One is electroplasticity [1-10], which controls the properties by applying pulsed electric current during deformation. The effect of EAM phenomena was first reported by Machlin [1] in 1959. According to Machlin, applying an electric current affects flow stress, ductility and yield strength of brittle rock salt. Thereafter, it has been reported that the mechanical behavior of various materials may be affected by applying high current density during deformation. Roth et al. [3] reported studies that achieved nearly 400% tensile elongation of aluminum 5754 alloys. Kim et al. [10] analyzed the microstructure changes after applying electric current during uniaxial tension and found that the electric current itself, rather than the Joule heating effect, was the dominant reason of annealing. Compared to conventional hot forming process, many researchers have reported that the applied electric current during deformation drastically affects the material properties such as yield stress, flow stress and elongation. Salandro et al. wrote a book put together

these studies on electrically assisted forming.

The other is electropulsing treatment [11-21], which controls microstructural change of a conductive metallic materials without deformation. Electropulsing treatment (EPT) is an effective technique that changes the microstructure of a metallic material and improves its physical properties by applying high electric current density at relatively low temperature. Conrad et al. [11-12] reported that the electric current itself could have an effect on the recrystallization kinetic of pure copper in addition to the well-known thermal effect by Joule heating. It was also suggested that the rate of recrystallization and recovery improved when the electric current was applied using the Arrhenius type equation. Zhou et al. [15] reported that the accelerated nucleation of phase transformation using electropulsing treatment for copper-zinc alloy was not caused by rapid heating or cooling rates but by electric current effect. this phenomenon was used in subsequent studies to obtain fine grained microstructures. In addition, the effect of electropulsing on microstructure ins not limited to recrystallization or phase transformation. Qin et al. [16] reported to be able to obtain a pearlite microstructure through EPT in the steel that cannot be obtained by the conventional heat treatment. To the present time, more and more researches on theses EAM phenomena have been conducted.

1.2 Hypotheses on electric current effect

After EAM phenomena have been reported, a lot of researches on the mechanism of electric current have been conducted. Magargee et al. [22] suggested that the phenomenon that flow stress decreased with continuous direct current during the uniaxial tension of pure titanium can be explained by only the Joule heating. When specimen was cooled at the same time as applying the electric current, tensile curve was similar to the curve of non-pulsed tensile test. However, the applied current density was 16 A/mm^2, which was considerably lower than the current density at which the EAM phenomena occurred. So, this alone cannot explain completely.

Some suggest that the movement of atoms was accelerated by electromigration [23-27]. Electromigration means that transport of material due to the continuous movement of ions in the conductor caused by the transfer of momentum between the conduction electrons and the scattered nuclei in the metal. Kozlova et al. [27] reported that breakage of Pd-Pt nanobridges occurred under a DC current of 3-5 x 10^5 A/mm^2. The electromigration effect can be dominant, because the kinetic energy of the electron becomes very large due to high current density in nanoscale structure such as an integrated circuit or a TEM sample. However, EAM phenomena of bulk metals occurs in the range of $10^{1\sim2}$ A/mm^2 in general, and electromigration alone is difficult to explain completely electric current effect.

There were attempts to explain the athermal effect of electric current as pinch

effect formed by the electromagnetic force or skin effect [26,28]. Pinch effect is that the Lorentz force generated when the electric current is applied causes a compressive force in the perpendicular direction of the current flow, and the movement of atoms is accelerated. Skin effect is that the current density is concentrated around the outer surface as the current density or frequency increases. The pinch effect or skin effect is also very insignificant in the current density range of EAM. In addition, the Skin effect does not appear under continuous direct current.

Recently, the suggestions of local Joule heating which means localized heating in defects such as grain boundary, dislocation which have high electrical resistivity accelerated the movement of atoms have been reported [29,30]. However, reports suggest only the possibility by calculation. So far, local Joule heating theory have not been proved experimentally. FEM calculation in author's research group showed that there was no temperature variation between the grain boundary and the matrix due to the high thermal conductivity when the electric current was applied to the microstructure.

The FEM calculation in author's group confirmed that the current density was concentrated at the grain boundaries when electric current was applied. In other words, it can be said that electric charge mainly was high near the grain boundaries. Through the first principle calculation, when additional electrons imposed on the microstructure including grain boundaries, large vibration of atoms near grain boundary was generated. This means that the application of electric current

weakens the atomic bonding near the defects like grain boundaries. When the elastic modulus was measured while applying electric current to aluminum alloys having different grain sizes, it was found that the amount of elastic modulus drop was much larger in the alloy having a small grain size (larger grain boundary area). Although the temperature did not actually increase near grain boundary, the atoms near the grain boundary acted as if the temperature had increased. As a result, the athermal effect of electric current can be explained in the way “effective temperature”.

1.3 Thesis motivation

It has been recognized that there is an athermal effect when applying an electric current. EAM is promising as next generation process because it can improve efficiency at lower temperature than thermo-mechanical process. However, mechanism is not fully understood so there is a difficulty in utilizing EAM because quantification of the athermal effect has not been established.

The objective of this study consisted of three parts. Firstly, the effect of electric current on recrystallization of low carbon steel is investigated based on JMAK (Johnson-Mehl-Avrami-Kolmogorov) kinetic analysis through microstructure observation and hardness measurement. This experimentally demonstrates results that electric current accelerates the movement of atoms. Second, it is investigated how the athermal effect changes as the current density changes based on the modified JMAK kinetic analysis. It is considered how the electric current affects acceleration of atomic diffusion by inserting the athermal effect term to the modified JMAK equation. Through these studies, the athermal effect of electric current is quantified with the concept of reducing the recrystallization activation energy or increasing the effective temperature.

Lastly, the results of the study are confirmed by calculation of the stress drop during electroplasticity using the quantitative athermal effect value. This provides an indication of applying electropulsing treatment technique to recrystallization process of low carbon steel.

1.4 Reference

[1] E.S. Machlin, Applied voltage and the plastic properties of`Brittle"rock salt, J. Appl. Phys. 30(7) (1959) 1109-1110.

[2] H. Conrad, Electroplasticity in metals and ceramics, Mater. Sci. Eng. A 287 (2000) 276-287.

[3] J.T. Roth, I. Loker, D. Mauck, M. Warner, S.F. Golovashchenko, A. Krause, Enhanced formability of 5754 alu11minum sheet metal using electric pulsing, Trans. NAMRI/SME. 36 (2008) 405-412.

[4] W.A. Salandro, J.J. Jones, T.A. McNeal, J.T. Roth, S.-T. Hong, M.T. Smith, Formability of Al 5xxx sheet metals using pulsed current for various heat treatments, J. Manuf. Technol. 132 (2010) 051016 1-11.

[5] N.T. Thien, N.T. Vinh, S.-T. Hong, M.-J. Kim, H.N. Han, F. Morestin, The effect of short duration electric current on the quasi-static tensile behavior of magnesium AZ31 alloy, Adv. Mater. Sci. Eng. Article ID 9560413.

[6] W.A. Salandro, A. Khalifa, J.T. Roth, Tensile formability enhancement of magnesium AZ31B-0 alloy using electrical pulsing, Trans. NAMRI/SME. 37 (2009) 387-394.

[7] R. Fan, J. Magargee, P. Hu, J. Cao, Influence of grain size and grain boundaries on the thermal and mechanical behavior of 70/30 brass under 405 electrically-assisted deformation, Mater. Sci. Eng. A-Struct. 574 (2013), 218–225.

[8] J. Magargee, F. Morestin, J. Cao, Characterization of flow stress for

commercially pure titanium subjected to electrically-assisted deformation. J. Eng. Mater. Technol. 135 (2013), 041003-1–041003-10.

[9] J. Magargee, R. Fan, J. Cao, Analysis and Observations of Current Density Sensitivity and Thermally Activated Mechanical Behavior in Electrically-Assisted Deformation, J. Manuf. Sci. Eng. 135 (2013), 061022-1-061022-8.

[10] M.-J. Kim, K. Lee, K.H. Oh, I.S. Choi, H.H. Yu, S.-T. Hong, H.N. Han, Electric current-induced annealing during uniaxial tension of aluminum alloy, Scr. Mater. 75 (2014) 58–61.

[11] H. Conrad, N. Karam, S. Mannan, Effect of electric current pulses on the recrystallization of copper, Scr. Metall. 17(3) (1983) 411-416.

[12] H. Conrad, N. Karam, S. Mannan, A. Sprecher, Effect of electric current pulses on the recrystallization kinetics of copper, Scr. Metall. 22(2) (1988) 235-238.

[13] Z.S. Xu, Y.X. Chen, Effect of electric current on the recrystallization behavior of cold worked α-Ti, Scr. Metall. 22(2) (1988) 187-190.

[14] G. Hu, G. Tang, Y. Zhu, C. Shek, Electropulsing induced texture evolution in the recrystallization of Fe-3 Pct Si alloy strip, Metall. Mater. Trans. A 42(11) (2011) 3484.

[15] Y. Zhou, J. Guo, W. Zhang, G. He, Influence of electropulsing on nucleation during phase transformation, J. Mater. Res. 17(12) (2002) 3012-3014.

[16] R. Qin, A. Rahnama, W. Lu, X. Zhang, B. Elliott-Bowman, Electropulsed steels, Mater. Sci. Technol. 30(9) (2014) 1040-1044.

[17] Y. Zhou, W. Zhang, B. Wang, J. Guo, Ultrafine-grained microstructure in

a Cu–Zn alloy produced by electropulsing treatment, J. Mater. Res. 18(8) (2003) 1991-1997.

[18] R. Fan, J. Magargee, P. Hu, J. Cao, Influence of grain size and grain boundaries on the thermal and mechanical behavior of 70/30 brass under electrically-assisted deformation, Mater. Sci. Eng., A 574 (2013) 218-225.

[19] J. Magargee, R. Fan, J. Cao, Analysis and observations of current density sensitivity and thermally activated mechanical behavior in electrically-assisted deformation, J. Manuf. Sci. Eng. 135(6) (2013) 061022.

[20] D. Ben, H. Yang, Y. Ma, X. Shao, J. Pang, Z. Zhang, Rapid hardening of AISI 4340 steel induced by electropulsing treatment, Mater. Sci. Eng., A 725 (2018) 28-32.

[21] Y. Ma, H. Yang, Y. Tian, J. Pang, Z. Zhang, Hardening and softening mechanisms in a nano-lamellar austenitic steel induced by electropulsing treatment, Mater. Sci. Eng., A 713 (2018) 146-150.

[22] J. Magargee, F. Morestin, J. Cao, Characterization of flow stress for commercially pure titanium subjected to electrically assisted deformation, J. Eng. Mater. Technol. 135 (2013) 041003.

[23] D. Xu, B. Lu, T. Cao, H. Zhang, J. Chen, H. Long, J. Cao, Enhancement of process capabilities in electrically-assisted double sided incremental forming, Mater. Des. 92 (2016) 268-280.

[24] H. Conrad, Thermally activated plastic flow of metals and ceramics with an electric field or current, Mater. Sci. Eng., A 322(1-2) (2002) 100-107.

[25] O. Troitskii, V. Likhtman, The Effect of the Anisotropy of Electron and Radiation on the Deformation of zinc single crystals in the Brittle State, Akaciemiya Nauk SSSR 147(4) (1963) 814-820.

[26] A. Sprecher, S. Mannan, H. Conrad, Overview no. 49: On the mechanisms for the electroplastic effect in metals, Acta Metall. 34(7) (1986) 1145-1162.

[27] T. Kozlova, M. Rudneva, and H. W. Zandbergen. In situ TEM and STEM studies of reversible electromigration in thin palladium-platinum bridges, Nanotechnology 24(50) (2013) 505708.

[28] E. Novillo, M.M. Petite, J.L. Bocos, A. Iza□Mendia, I. Gutiérrez, Texture and Microtexture Evolution in an Ultra□Low Carbon Steel During Recrystallization, Adv. Eng. Mater. 5(8) (2003) 575-578

[29] L. Dong, S. Youkey, J. Bush, V. M. Dubin, J. Jiao, and R. V. Chebiam, Effects of local Joule heating on the reduction of contact resistance between carbon nanotubes and metal electrodes, J. Appl. Phys. 101 (2007) 024320

[30] T. B. Holland, U. A. Tamburini, D. V. Quach, T. B. Tran, and A. K. Mukherjee, Effects of local Joule heating during the field assisted sintering of ionic ceramics, J. Eur. Ceram. Soc. 32 (2012) 3667-3674.

Chapter 2

Recrystallization kinetic changes with applying electric current of low carbon steel

2.1 Introduction

In the research area of structural materials, heat treatment is significantly important to improve mechanical properties such as ductility, strength, toughness, etc. Many researchers have studied various heat treatment methods to obtain microstructures having better mechanical properties. However, the conventional heat treatment using a furnace is time-consuming and requires heating at a certain temperature. This may cause problems such as oxidation, surface deterioration, and grain growth, which hinder the material property. Thus, an effective method is needed to control the microstructure to ensure a sound material property.

Since the first report in 1959, many studies have indicated that electric current can influence the mechanical and microstructural behavior of materials [1]. Applying a high density electric current to a material without deformation, which is often called electropulsing treatment (EPT), has been suggested to be an effective method to control the microstructures of the material [2-11]. Conrad *et al*. [2,3] reported that the electric current strongly affected the recrystallization kinetics of pure copper. Chen *et al*. [4] reported that the formation of intermetallic compounds

was promoted when the electric current was applied to the interface between Sn/Cu and Sn/Ni. Xu *et al*. [5] reported that the recrystallization and grain growth of cold-rolled α-Ti were accelerated by applying electric current. Bertolino *et al*. [6] reported that the interface reaction of an Au-Al multilayer became active when applying electric current. Wang *et al*. [7] found that the electric current affected the dendrite growth of a solidifying Sn/Pb bi-alloy through in-situ observation. Recently, the authors [8] reported that the dissolution of $Mg_{17}Al_{12}$ intermetallic phase was accelerated by electropulsing treatment in AZ91 alloy.

As for the effect of electric current, some researchers have suggested that it can be explained just by the thermal effect due to Joule heating [12,13]. Magargee *et al*. [13] showed that the mechanical behavior of commercially pure titanium during electrically assisted deformation could be effectively predicted based on a thermo-mechanical constitutive model reflecting the thermal effect due to Joule heating. On the other hand, some researchers have suggested that the effect of electric current cannot be fully explained by only considering the thermal effect [14-20]. Lin *et al*. [14] reported that the dynamic recrystallization temperature was obviously decreased under the electric current for AZ31 alloy. Recently, the authors have observed the athermal effects of electric current during deformation [16-20]. The elongation of AA5052 alloy increased drastically by applying pulsed electric current during the tensile test, and this was related to electric current induced annealing by dislocation annihilation with different effects from Joule heating [16,17]. The authors also reported that electric current-assisted aging occurred

rapidly during deformation at relatively low temperatures compared to conventional aging condition in AA6061 alloy [18]. These studies suggest that microstructural change can be accelerated by applying electric current separate from the effect of Joule heating. However, hypotheses about the athermal effect of electric current have limits.

In this chapter, the effect of electric current on recrystallization kinetics was investigated for work-hardened interstitial free (IF) steel. The annealing process was carried out through the EPT and the conventional heat treatment (HT) using a furnace. The recrystallization kinetics was analyzed by using Vickers hardness tests and microstructural observation. In addition, the effect of electric current on recrystallization kinetics was quantitatively evaluated by adopting the Johnson-Mehl-Avrami-Kolmogorov (JMAK) equation.

2.2 Experimental procedure

2.2.1 Specimen preparation

A IF steel (Fe-0.001C-0.2Mn-0.02Nb in wt.%) was used in this study because this material was single phase and few alloying elements that affect microstructure change were added. It was cold rolled up to 80%. The initial microstructure is shown as deformed structure in Fig. 2.1.

The EPT was carried out using a power supply (SPS, Eltech Inc., Republic of Korea), which can apply a DC pulse of up to 4000 A at a frequency of 20000 Hz to control the temperature of the specimen. As shown in Fig. 2.2, for the EPT experiment, a disk-shaped specimen was inserted between the two graphite electrodes. The specimen was prepared to have a diameter of 10 mm and a thickness of 1 mm. A conductive sheet was placed between the specimen and the electrodes to prevent carburization from the graphite electrodes. The contact pressure was 20 MPa. The temperature rise due to Joule heating upon application of electric current was measured using K-type thermocouple and infrared camera. EPT was conducted at two heating modes: (i) for fixed annealing time at different annealing temperatures and (ii) at fixed annealing temperature for different annealing times. In the case of mode (i), the annealing temperature was set at 600-700℃ with a 10℃ interval at the fixed annealing time of 60 sec. In order to obtain the annealing temperature corresponding to each material, the current density of 12 to 21 A/mm^2 were applied. In mode (ii), the annealing times were 0.5, 60, 90, 120, 180, 720, and 960 sec at the fixed annealing temperature of 610℃. The heating rate

was 1.67℃/sec and the vacuum level of the chamber during the entire experiment was maintained below 10^{-3} torr. Following EPT, the specimen was removed from the vacuum chamber, and then air cooled to room temperature.

In order to exclude the thermal effect of temperature rise, the HT was conducted using a resistance heating furnace (Lindberg, Thermo Electron Corporation, USA) in a similar temperature history to EPT. A K-type thermocouple was attached to the specimen and the temperature of the specimen was measured in real time for HT.

Vickers hardness was measured to quantitatively compare the hardness changes of the specimens according to the treatment conditions. The experiment was repeated 10 times for each specimen for reproducibility. The measurement load was set to HV 3.

The microstructure was observed by using a field emission gun scanning electron microscope (FE-SEM, SU70, Hitachi, Japan) equipped with an electron backscatter diffraction system (EBSD, EDAX/TSL, Hikari, USA). The specimens were mechanically polished to 1 μm and electropolished using 10% perchloric acid and 90% ehanol solution. For the EBSD analysis, an acceleration voltage of 15 kV was used. The critical misorientation angle of 10^{o} was set for grain identification.

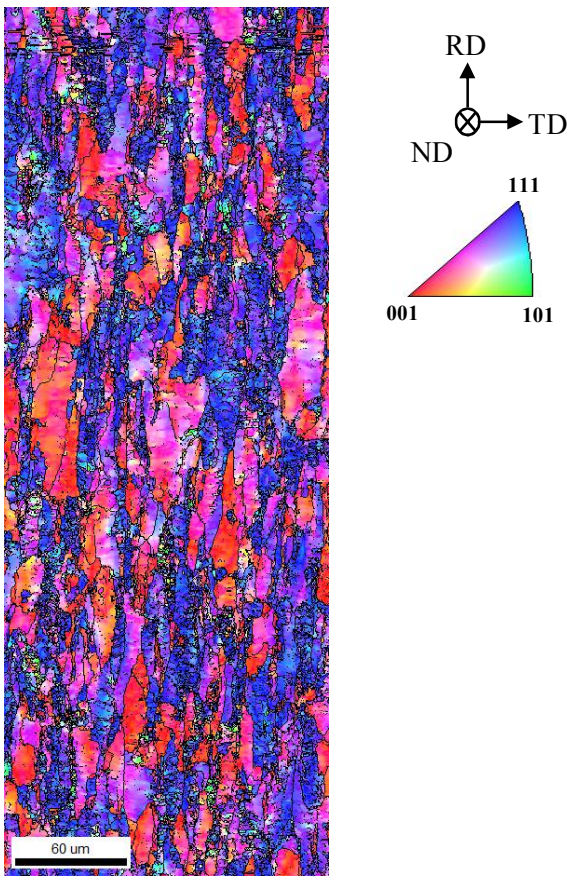

Figure 2.1 EBSD inverse pole figure map of normal direction for initial specimen

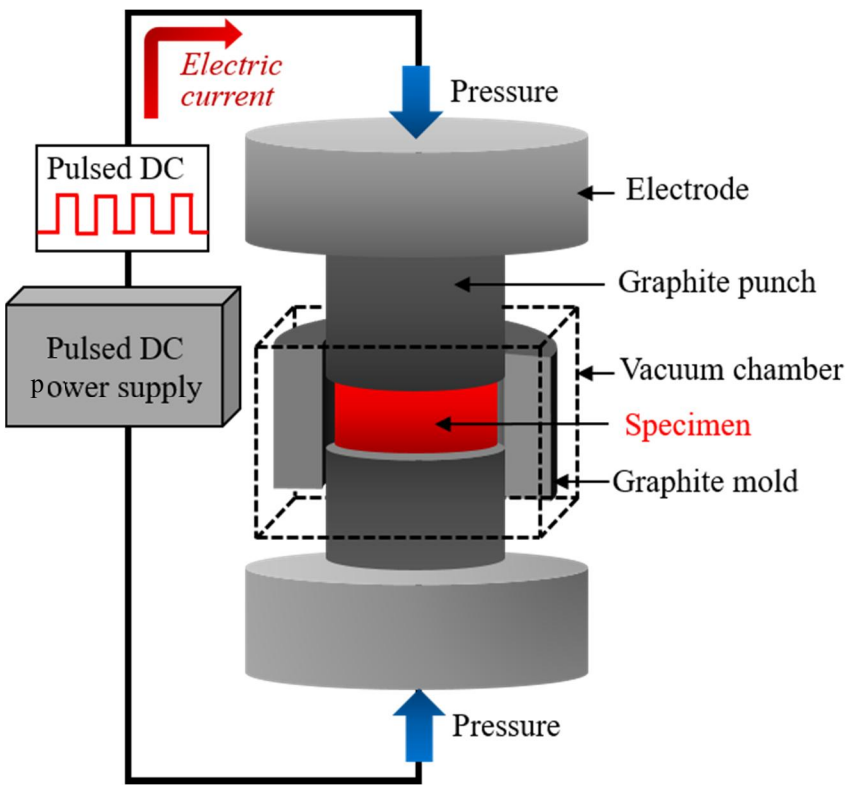

Figure 2.2 Schematic of the electropulsing treatment (EPT) equipment

2.3 Vickers hardness change according to EPT

The annealing process of IF steel was studied by using the measurements of Vickers hardness as shown in Fig. 2.3. The Vickers hardness of the specimen before annealing (hereafter "initial specimen") is about 200 HV, as shown in Fig. 2.3 (a). At a fixed annealing time of 60 sec, it was observed that the hardness decreases with increasing annealing temperature in both EPT and HT. The hardness started to decrease at 620℃ under EPT, while it started to decrease at 670℃ under HT. Also, the hardness values were asymptotic with further increases at annealing temperature over 660℃ in EPT, while it remained constant at the annealing temperature of over 760℃ in HT. At the annealing temperature of 660℃, the hardness was 88.2 HV in EPT, while it was still 203.6 HV in HT indicating negligible annealing effects compared with the initial specimen. Note that the temperature at which the hardness was asymptotic with further increases is about 100℃ lower in EPT than in HT at the fixed annealing time of 60 sec.

The hardness value was also measured as a function of annealing time at a fixed annealing temperature of 620℃ as shown in Fig. 2.3 (b). In EPT, it was difficult to predict the point where the hardness first decreases due to the rapid reduction of hardness even in the short annealing time of 20 sec. In HT, the hardness value began to decrease within 250 sec. At the annealing time of 720 sec, the hardness value became at 100 HV in EPT, whereas it was still a higher value at 175 HV in HT. The hardness value in the HT was finally lowered to 100 HV after 64,000 sec. the time required for the hardness reduction in the HT was more than

88 times slower than that in EPT. The significantly lower hardness value in EPT compared to HT at the fixed annealing temperature (Fig. 2.3 (a)) or the annealing time (Fig. 2.3 (b)) in the IF steel supports the hypothesis that annealing may be accelerated by EPT due to the athermal effect of electric current.

The decrease in hardness occurred at a lower temperature at the fixed annealing time and in a shorter period of time at the fixed temperature in EPT compared to HT. Verification of annealing based on microstructural observation is discussed in detail in section 2.4.

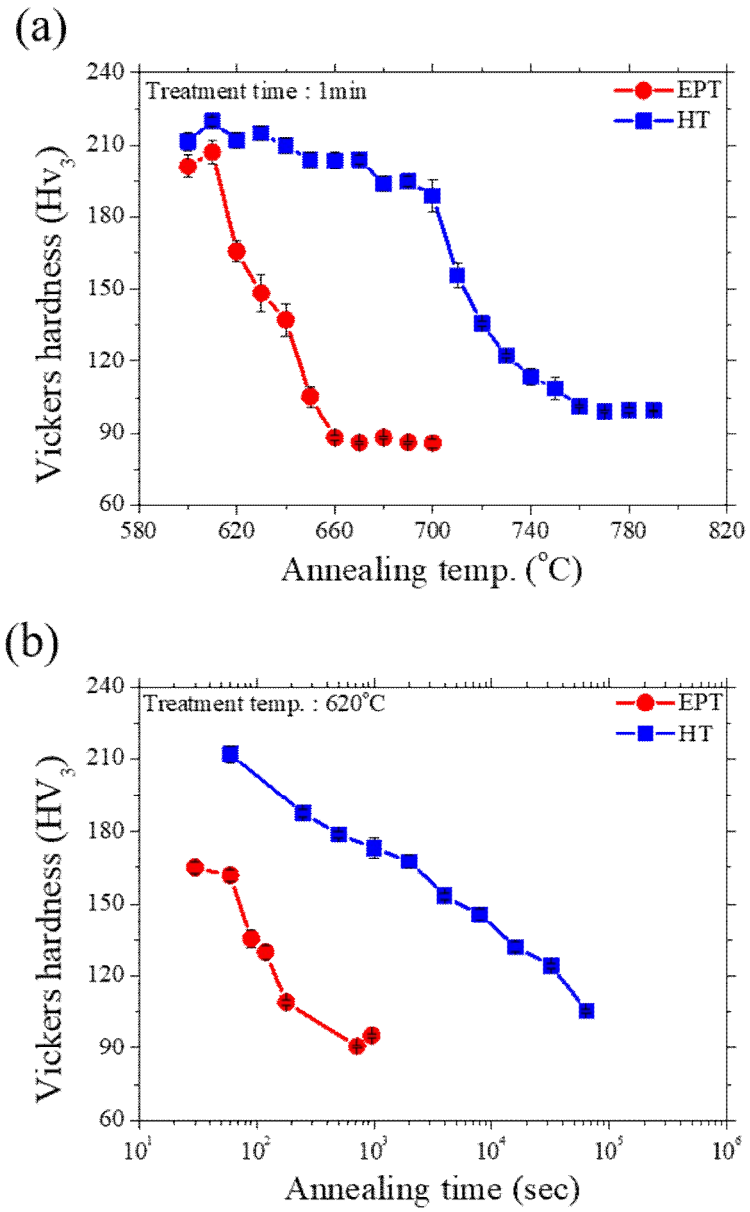

Figure 2.3 Vickers hardness of electropulsing treatment (EPT, red circle) and heat treatment (HT, blue square) versus (a) for 60 sec under various temperatures and (b) at 620℃ for various annealing times

2.4 Microstructure change according to EPT

Microstructural analysis was conducted to verify the effect of electric current causing the rapid decrease of hardness for the IF steel. At the fixed annealing time of 60 sec, the microstructure after EPT at 630℃ consists of a large amount of non-recrystallized grains with a few recrystallization nuclei, as shown in Fig. 2.4 (a). Similarly, a bimodal microstructure involving a large amount of non-recrystallized grains and a few recrystallization nuclei were observed after HT at 710℃, as shown in Fig. 2.4 (c). For the annealing condition in EPT at 630℃ and HT at 710℃, the hardness values were close to 150 HV (Fig. 2.3 (a)). At the hardness value of about 100 HV, the fully recrystallized grains were observed after EPT at 660℃ and HT at 760℃ for 60 sec (Figs. 2.4 (b) and 2.4 (d)). Grain size after EPT at 660℃ and HT at 760℃ for 60 sec were almost the same as 12 μm and 11 μm, respectively, with an equiaxed shape. This result suggests that the characteristics of the recrystallized grains including grain shape and grain size after EPT did not differ from that of the recrystallized grain structure after HT. Note that the recrystallization was fully completed at 660℃ in EPT as shown in Fig. 2.4 (b), while large amounts of deformed grains remained after HT, as shown in Fig. 2.4 (c) even at the higher annealing temperature of 710℃ compared to EPT.

From the results of hardness analysis and microstructure, it is confirmed that the reduced hardness value was caused by recrystallization. The annealing temperature required for full recrystallization through EPT was lower than HT at the fixed annealing time. Also, a shorter annealing time for full recrystallization in

EPT was required compared to HT at the fixed annealing temperature. This implies that an electric current might accelerate the recrystallization with an effect distinct from Joule heating.

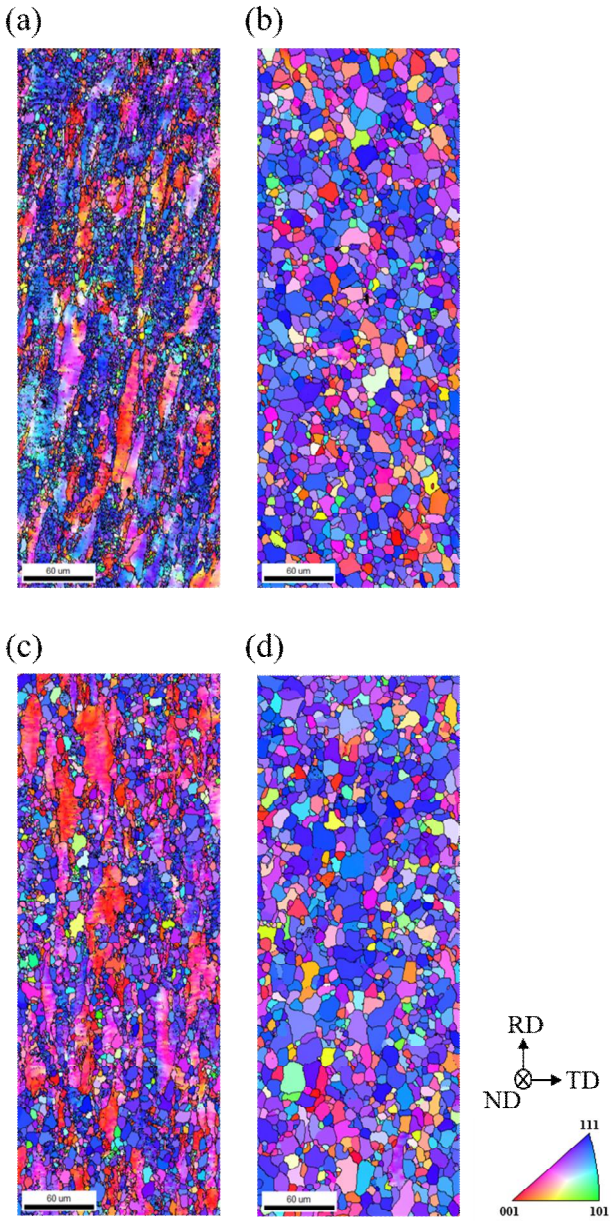

Figure 2.4 EBSD inverse pole figure maps of normal direction (ND) for IF steel obtained from (a) EPT at 630℃, (b) ETP at 660℃, (c) HT at 710℃ and (d) HT at 760℃ for 60 sec

2.5 Recrystallization kinetic analysis

The relationship between recrystallization fraction (x_r) and annealing time (t) can be described by the Johnson-Mehl-Avrami-Kolmogorov (JMAK) equation [21-24].

$$x_r = 1 - exp(-kt^n) \quad (2.1)$$

Where k is an avrami kinetic constant, and n is an Avrami exponent, which varies depending on the nucleation rate and type of grain growth. The grain orientation spread (GOS) of EBSD was used to determine the recrystallization fraction and the recrystallized grain is defined within 1° of GOS [25]. The change in the recrystallization fraction in EPT and HT depending on annealing time at 620℃ is represented in Fig. 2.5. In the EPT (Figs. 2.5 (a) – 2.5 (d)), recrystallization began to occur more rapidly than in the HT, and recrystallization was almost completed after 960 sec. In the HT, recrystallization hardly occurred even after 1,000 sec, and was completed after 64,000 sec. The recrystallization fraction versus annealing time was fitted to Eq. (1), as shown in Figs. 2.6 (a). The values of k and n were obtained by fitting the data for $ln(-\ln(1-x))$ and $ln(t)$ (Fig. 2.6 (b)). The values of n are listed in Table. 2.1. The Avrami exponent n varies in the range of from 0.5 to 4 depending on the nucleation rate [20]. n is 0.78 in EPT which is relatively higher than that of 0.62 in HT. This implies that electric current affects the nucleation rate with an effect distinct from Joule heating.

The time t_{50} required for the hardness to reach the mid-value between the hardness of deformed and recrystallized specimens was taken as the rate parameter

to evaluate the effect of the electric current on the recrystallization kinetics (Fig. 2.3). In the case of the IF steel, it was confirmed that 34% recrystallization proceeded on mid-value of hardness in both EPT and HT through GOS analysis of EBSD. The average grain size of the recrystallized grains was 11 μm. The relationship between time and temperature is expressed as the Arrhenius equation (2.2) [2,3,26].

$$1/t_{50} = Aexp(-Q/RT) \quad (2.2)$$

where $1/t_{50}$ is the rate constant (s^{-1}) at T (K), A is the pre-exponential constant (s^{-1}), R is gas constant (J/k·mol), and Q is the activation energy (J/mol) required for recrystallization under EPT and HT. Plots of $1/t_{50}$ and $1/T$ for mid-value of hardness under EPT and HT are given in Fig. 2.7, and the calculated activation energies are shown in Table. 2.1. Using activation energy and k obtained from Figs. 2.6 (b) and 2.6 (d), k_0 is also derived based on the following equation (2.3) and listed in Table 2.1.

$$k = k_0 exp(-Q/RT) \quad (2.3)$$

The activation energy of the IF steel in HT was calculated as 443 kJ/mol, which is similar to the values from the literature [27]. In the case of EPT, the activation energy of 366 kJ/mol was obtained, which is clearly lower than the activation energy in HT. It was thus found that the activation energy for recrystallization in EPT is lower than that in HT. This means that the rate of recrystallization kinetics was increased by the reduction of the activation barrier due to the athermal effect of electric current. However, since the precise

recrystallization activation energy is likely to be a function of the electric current density, the activation energy value obtained in EPT may be only regarded as an effective value for the range of the given electric current densities used in the present study. Further studies are needed to more precisely describe the recrystallization activation energy in EPT as a function of the electric current density.

When the electric current was applied to the IF steel in the annealing process, it was possible to reduce the annealing temperature and time for recrystallization with an athermal effect distinct from Joule heating. It is identified that electric current may affect the nucleation rate and reduce the activation energy for recrystallization. This study demonstrates that EPT can reduce process time in the recrystallization process due to the athermal effect of electric current.

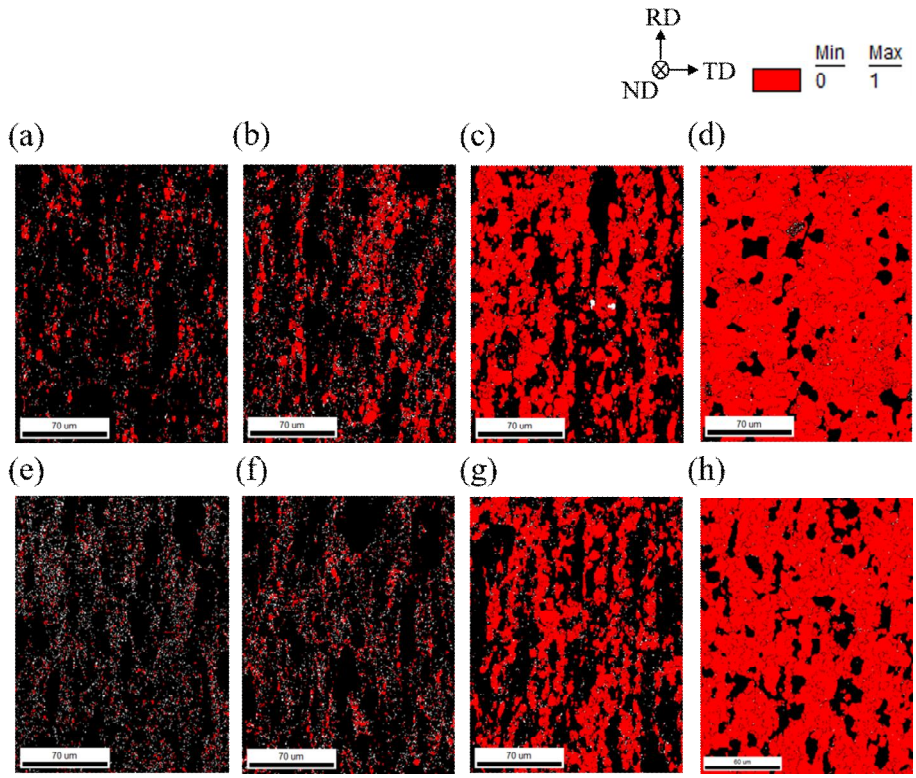

Figure 2.5 EBSD grain orientation spread maps of normal direction (ND) for EPT at 620℃ for (a) 15 sec, (b) 60 sec, (c) 240 sec, (d) 960 sec, for HT at 620℃ for € 250 sec, (f) 1000 sec, (g) 16,000 sec and (h) 64,000 sec

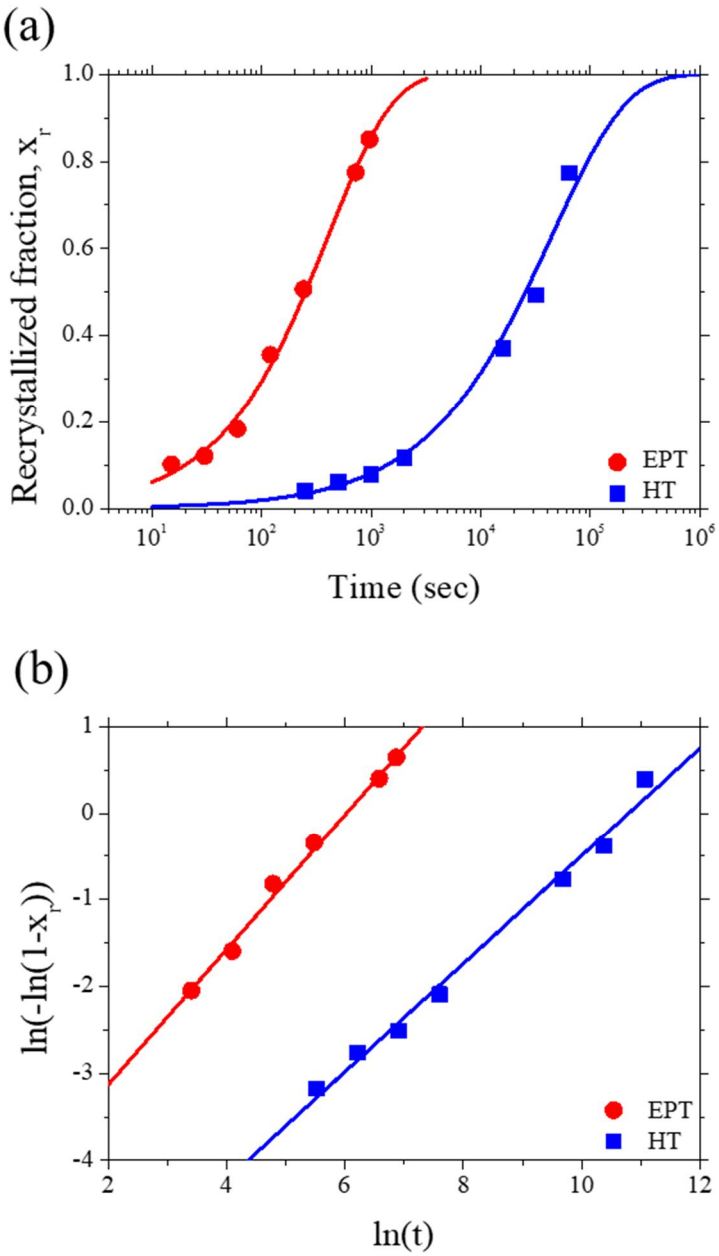

Figure 2.6 (a) Recrystallization fraction versus annealing time at annealing temperature of 620℃ and (b) JMAK plots with fitted line (solid)

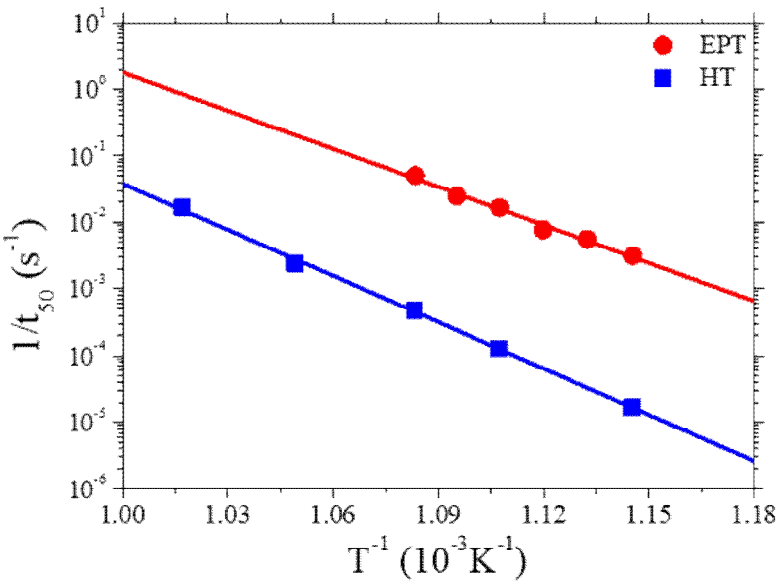

Figure 2.7 The Arrhenius plots of EPT and HT with fitted line (solid)

Table 2.1 Parameters of JMAK equation for EPT and HT.

	Q	n	k_0
Electropulsing treatment (EPT)	366.1	0.78	0.0098
Heat treatment (HT)	433.8	0.62	0.0013

2.6 Conclusion

The effect of electric current on recrystallization kinetics in work-hardened IF steel was investigated by electropulsing treatment (EPT) and furnace heat treatment (HT). From the Vickers hardness analysis, the hardness value after EPT is clearly lower than that after HT at the same annealing condition. Based on the microstructural analysis, it was confirmed that the reduced hardness value is caused by recrystallization. These results support that a lower annealing temperature and shorter annealing time are needed in EPT compared to HT. They also imply that electric current might accelerate the recrystallization with the athermal effect distinct from Joule heating. To identify the athermal effect of electric current on recrystallization kinetics, the Johnson-Mehl-Avrami-Kolmogorov (JMAK) equation was adopted. The value of the Avrami exponent, which is related to the nucleation rate for recrystallization, is relatively higher in EPT than in HT. Also, the activation energy of IF steel in EPT is 366 kJ/mol, which is lower than that in HT. Therefore, it is found that electric current might reduce the activation energy for recrystallization with the athermal effect distinct from Joule heating. The study provides significant insight into the area of heat treatment of materials. By using EPT, it was possible to reduce the annealing temperature and time for recrystallization compared to conventional heat treatment using a furnace.

2.7 References

[1] E.S. Machlin, Applied Voltage and the Plastic Properties of "Brittle" Rock Salt, Journal of Applied Physics 30 (1959) 1109-1110.

[2] H. Conrad, N. Karam, S. Mannan, A. Sprecher, Effect of electric current pulses on the recrystallization kinetics of copper, Scripta Metallurgica 22 (1988) 235-238.

[3] H. Conrad, N. Karam, S. Mannan, Effect of electric current pulses on the recrystallization of copper, Scripta Metallurgica 17 (1983) 411-416.

[4] S.-W. Chen, C.-M. Chen, W.-C. Liu, Electric current effects upon the Sn/Cu and Sn/Ni interfacial reactions, Journal of Electronic Materials 27 (1998) 1193-1199.

[5] Z.S. Xu, Y.X. Chen, Effect of electric current on the recrystallization behavior of cold worked α-Ti, Scripta Metallurgica 22 (1988) 187-190.

[6] N. Bertolino, J. Garay, U. Anselmi-Tamburini, Z. Munir, High-flux current effects in interfacial reactions in Au–Al multilayers, Philosophical Magazine B 82 (2002) 969-985.

[7] T. Wang, J. Xu, T. Xiao, H. Xie, J. Li, T. Li, Z. Cao, Evolution of dendrite morphology of a binary alloy under an applied electric current: An in situ observation, Physical Review E 81 (2010) Article ID 042601.

[8] H.-J. Jeong, M.-J. Kim, J.-W. Park, C.D. Yim, J.J. Kim, O.D. Kwon, P.P. Madakashira, H.N. Han, Effect of pulsed electric current on dissolution of Mg17Al12 phases in as-extruded AZ91 magnesium alloy, Materials Science

and Engineering A 684 (2017) 668-676.

[9] R. Fan, J. Magargee, P. Hu, J. Cao, Influence of grain size and grain boundaries on the thermal and mechanical behavior of 70/30 brass under 405 electrically-assisted deformation, Materials Science and Engineering A-Structural Materials Properties Microstructrue and Processing 574 (2013), 218–225.

[10] J. Magargee, R. Fan, J. Cao, Analysis and Observations of Current Density Sensitivity and Thermally Activated Mechanical Behavior in Electrically-Assisted Deformation, Journal of Manufacturing Science and Engineering 135 (2013), Article ID 061022-1-061022-8.

[11] J.T. Roth, I. Loker, D. Mauck, M. Warner, S.F. Golovashchenko, A. Krause, Enhanced formability of 5754 aluminum sheet metal using electric pulsing, Transactions of the North American Manufacturing Research Institution of SME 36 (2008) 405-412.

[12] C. Li, S. Jiang, K. Zhang, Pulse current-assisted hot-forming of light metal alloy, International Journal of Advanced Manufacturing Technology 63 (2012) 931-938.

[13] J. Magargee, F. Morestin, J. Cao, Characterization of flow stress for commercially pure titanium subjected to electrically assisted deformation, Journal of Engineering Materials and Technology 135 (2013) Article ID 041003.

[14] S. Lin, X. Chu, W. Bao, J. Gao, L. Ruan, Experimental investigation of pulse current on mechanical behaviour of AZ31 alloy, Journal of Engineering

Materials and Technology 31 (2015) 1131-1138.

[15] K. Huang, C. Cayron, R.E. Logé, The surprising influence of continuous alternating electric current on recrystallization behaviour of a cold-rolled Alumisium alloy, Materials Characterization 129 (2017) 121-126.

[16] M.-J. Kim, K. Lee, K.H. Oh, I.-S. Choi, H.-H. Yu, S.-T. Hong, H.N. Han, Electric current-induced annealing during uniaxial tension of aluminum alloy, Scripta Materiallia 75 (2014) 58-61.

[17] J.-H. Roh, J.-J. Seo, S.-T. Hong, M.-J. Kim, H.N. Han, J.T. Roth, The mechanical behavior of 5052-H32 aluminum alloys under a pulsed electric current, International Journal of Plasticity 58 (2014) 84-99.

[18] M.-J. Kim, M.-G. Lee, K. Hariharan, S.-T. Hong, I.-S. Choi, D. Kim, K.H. Oh, H.N. Han, Electric current–assisted deformation behavior of Al-Mg-Si alloy under uniaxial tension, International Journal of Plasticity 94 (2017) 148-170.

[19] Y.J. Lee, H.-M. Sung, Y. Jin, K. Lee, C.R. Park, G.-H. Kim, H.N. Han, Improvement of mechanical property of air plasma sprayed tungsten film using pulsed electric current treatment, International Journal of Refractory Metals Hard Matererials 60 (2016) 99-103.

[20] J.-I. Kim, S.-W. Jin, J. Jung, H.-M. Sung, H.-J, Jeong, S. Park, J.-W. Park, H.N. Han, Growth behavior of intermetallic compound in Al-Cu dissimilar conductor joint under direct current, Korean Journal of Metals and Materials 55 (2017) 372-378.

[21] W. Ye, R. Le Gall, G. Saindrenan, A study of the recrystallization of an IF steel

by kinetics models, Materials Science and Engineering A 332 (2002) 41-46.

[22] N. Sun, X. Liu, K. Lu, An explanation to the anomalous Avrami exponent, Scripta Materiallia 34 (1996) 1201-1207.

[23] F. Humphreys, A unified theory of recovery, recrystallization and grain growth, based on the stability and growth of cellular microstructures—I. The basic model, Acta Materiallia 45 (1997) 4231-4240.

[24] J. Kohout, An alternative to the JMAK equation for a better description of phase transformation kinetics, Journal of Materials Science 43 (2008) 1334-1339.

[25] L. Bracke, K. Verbeken, L. Kestens, J. Penning, Microstructure and texture evolution during cold rolling and annealing of a high Mn TWIP steel, Acta Materiallia 57 (2009) 1512-1524.

[26] Y. Lü, D.A. Molodov, G. Gottstein, Recrystallization kinetics and microstructure evolution during annealing of a cold-rolled Fe–Mn–C alloy, Acta Materiallia 59 (2011) 3229-3243.

[27] J. Go, Recovery and recrystallization behaviour of AA5754 and IF-Boron steel during annealing, University of British Columbia (2001).

[28] J. Shi, K. Cui, B. Wang, L. Deng, C. Wang, Z. Xu, Q. Li Effect of initial microstructure on static recrystallization of Mg-3Al-1Zn alloy, Materials Characterization 129 (2017) 104-113.

[29] H. Miradeh, A comparative study on the hot flow stress of Mg-Al-Zn magnesium alloys using a simple physically-based approach, Journal of

Magnesium and Alloys 2 (2014) 225-229.

Chapter 3

Effect of electric current density on recrystallization kinetic

3.1 Introduction

Annealing is one of the important heat treatments, which involves recovery and recrystallization processes to eliminate the residual stress and improve the mechanical properties such as ductility and toughness of the material. Various heating methods for annealing have been studied to control the microstructure more effectively and obtain better mechanical properties [1,2]. However, the conventional heating methods are generally time-consuming and may cause problems such as surface oxidation, thermal degradation, and inhomogeneous temperature distribution on the material. Therefore, alternative methods are needed to make up for these shortcomings and obtain improved mechanical properties of the materials.

In this regard, applying electric current has been known to be an effective way as it can anneal materials in a very short time and significantly accelerate the recrystallization kinetics of materials as compared to conventional heat treatment [3-6]. Since it has been reported for the first time that electric current can affect the mechanical properties of the material [7], various researches have been devoted to

investigating the effect of applying electric current on the materials. Many studies have demonstrated that the applied electric current during deformation of material can alter the material properties such as yield stress, flow stress, and elongation [8-17]. In addition, it has been shown that the microstructure of materials can be effectively controlled by electropulsing treatment (EPT), also known as electric current pulse (ECP) treatment, in which the electric current pulse is applied to the material even under conditions where no deformation occurs [3,4,6,18-25].

When it comes to the effect of the electric current on the materials, several studies have suggested that the phenomena can be explained only by a thermal effect due to Joule heating [26,27]. However, numerous studies have reported that the thermal effect is insufficient to fully account for the electric current effect, and there is an additional athermal effect distinct from the Joule heat generated during the EPT [5,8,9,15,28-36]. To elucidate the mechanism of the athermal effect of the electric current, theories such as electron wind [6,29,37-39], electrostatic field [40,41], skin effect and pinch effect [42], and magnetic effects [43] have been proposed. More recently, a study has demonstrated that the athermal effect is due to the charge imbalance near the grain boundaries under the electric current. Despite these researches, there is still a lack of scientific understanding of the EPT. Moreover, few attempts have been made to quantify the athermal effect.

In this chapter, athermal effect of electric current during recrystallization of low carbon steel was investigated and quantified through the single pulse treatment (SPT). We examined the changes of the microstructure, Vickers hardness, and the

amount of recrystallization while applying single current pulse with various electric current densities and duration times. The annealing process through conventional furnace treatment (CFT) was also carried out to exclude thermal effect in comparison with SPT. By conducting this comparative experiment, we clarified the athermal effect distinguished from the thermal effect due to Joule heating. The athermal effect was described by evaluating the recrystallization fraction of the material using EBSD analysis. In order to quantify athermal effect of electric current density, modified Johnson-Mehl-Avrami-Kolmogorov (JMAK) equation adopting the additivity rule and introducing effective value concept was used. Relevant parameters required for the equation were determined through optimization using a genetic algorithm (GA). Through this process, we intended to correlate the electric current density with the athermal effect.

3.2 Materials and methods

3.2.1 Experimental procedure

The material used in this study is ultra-low carbon steel sheet (Fe-0.005C-0.05Si-0.08Mn-0.011P-0.04Ti-0.06Al in wt.%), which has extra deep drawing quality (EDDQ). In order to evaluate recrystallization behavior, the material was first cold rolled up to 80% reduction of thickness. Specimen was fabricated to be 40 mm in the rolling direction (RD), 10 mm in the transverse direction (TD), and 0.6 mm in the normal direction (ND).

Application of electric current was performed using two power supplies. Below the electric current of 400 A, a customized power supply (Weltech, Republic of Korea) was used. Above 400 A, a power supply converted from a resistance welding controller (Vadal SP-1000U, Hyosung, Republic of Korea). A stage was constructed as shown in Fig 3.1 to apply the electric current to the specimen. The electric current was applied in parallel direction with the RD of the specimen. One of two holders was designed to be placed on the lubricated rail that is able to move to prevent bending of the specimen, which can be caused by thermal expansion of the holder when the electric current was applied. The intensity of the electric current actually applied to the specimen was measured using a clamp meter (PAC 22, Chauvin Arnoux, France). As shown Fig. 3.2, only one pulse of the electric current was applied to the specimen. The applied current densities were set to 40, 50, 68, 140, and 210 A/mm^2. The preset current density was applied and the pulsing time was accordingly set to certain value so that the peak annealing

temperatures by the SPT to be 700, 760, 800, and 860℃, as described in Table 3.1.

The temperature of the specimen was measured using an infrared thermal imaging camera (FLIR T430, FLIR Systems, Sweden). Black thermal paint is sprayed on the top of the specimen, and emissivity is calibrated using a K-type thermocouple. The temperature histories measured during the EPTs with various current densities to reach the respective target peak temperatures are shown in Fig. 3.3.

In order to exclude the thermal effect by Joule heating, CFT of the specimens was conducted using a resistance heating furnace (Lindberg/Blue M, Thermo Electron, USA). A K-type thermocouple was welded to the specimen for the temperature measurement. To obtain a rapid heating rate similar to the SPT process, the furnace was set to 1200℃ during the CFT process, which was the maximum possible setting temperature. When the temperatures of the specimens reached the desired target of 800, 850, 870, and 900℃, respectively, the specimens were taken out and air-cooled. The temperature histories measured during the HT were shown in Fig. 3.4

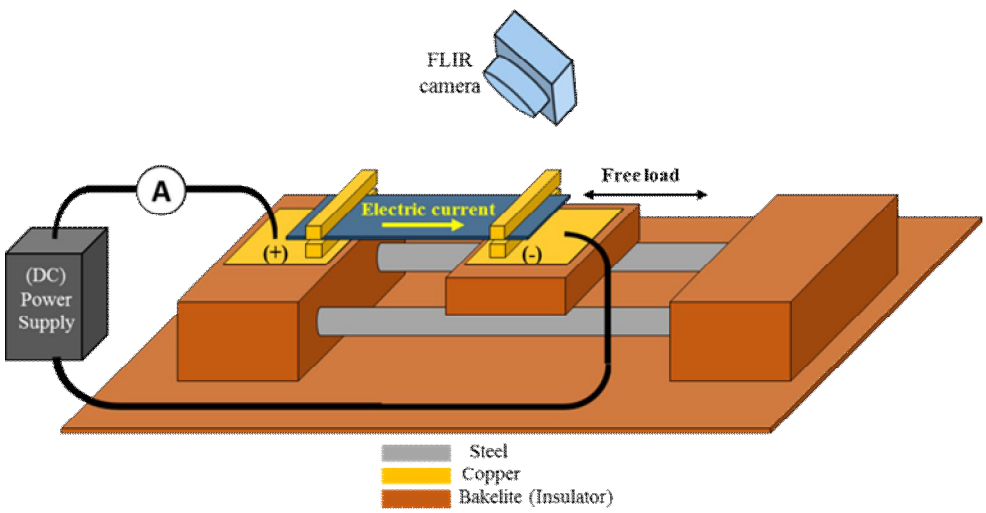

Figure 3.1 Instrumental set-up for single pulse treatment (SPT)

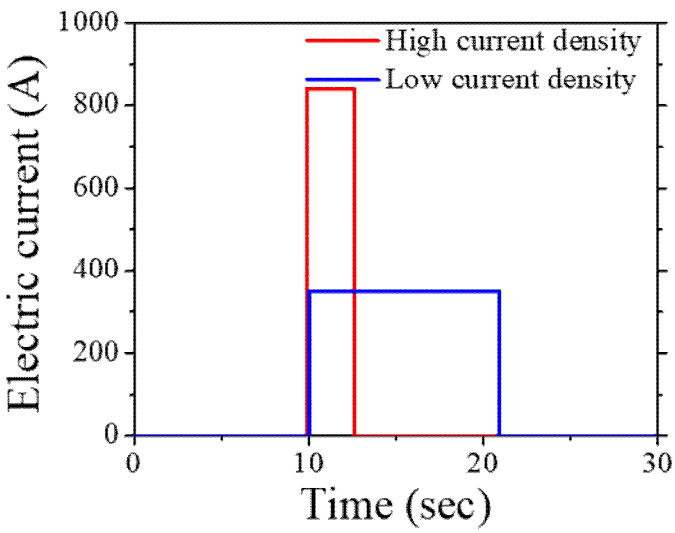

Figure 3.2 Schematic of SPT conditions applied to the specimen

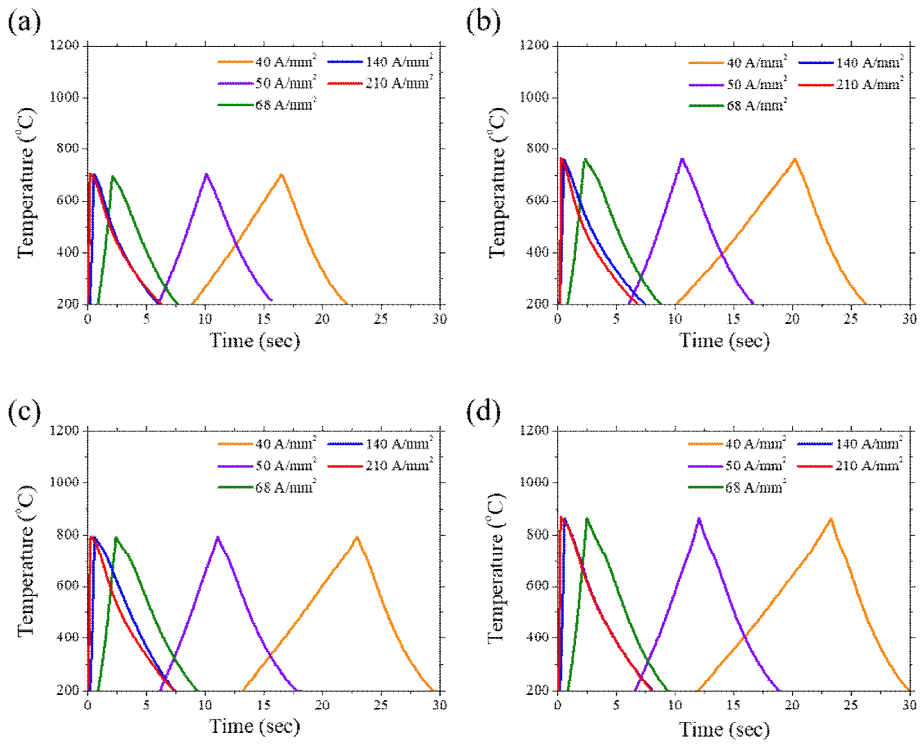

Figure 3.3 Temperature histories measured during the SPT with different current densities to reach the target peak temperatures of (a) 700℃, (b) 760℃, (c) 800℃ and (d) 860℃

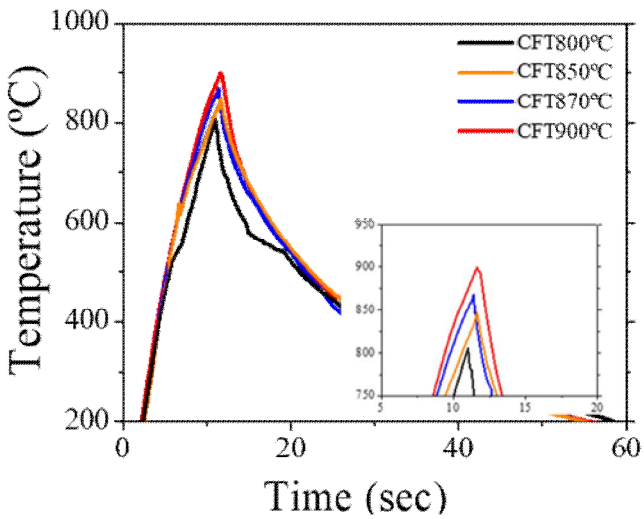

Figure 3.4 Temperature histories measured during the CFT and highlight of peak temperature

Table 3.1 Pulsing conditions each peak temperature

Peak temperature (℃)	Electric current density (A/mm^2)				
	Duration (sec)				
700	40	50	68	140	210
	0.23	0.523	2.1	10.09	16.5
760	40	50	68	140	210
	0.24	0.545	2.25	10.56	20.2
800	40	50	68	140	210
	0.25	0.56	2.4	11.06	22.93
860	40	50	68	140	210
	0.26	0.584	2.45	12.04	23.28

3.2.2 Microstructure observation

For microstructure observation, the specimens were polished to a diamond suspension of 1 μm, and then electro-polished with 10% perchloric acid and 90% ethanol solution at 20 V on the ND plane of the specimen. The microstructure of the specimens was characterized by a field emission gun scanning electron microscope (FE-SEM, SU70, Hitachi, Japan) equipped with electron backscatter diffraction (EBSD) system (EDAX/TSL, Hikari, USA). The specimens were scanned under an accelerating voltage of 15 kV and a working distance of 15 mm with a tilted angle of 70°. Post-processing was carried out using TSL OIM Analysis 6 software. The critical misorientation angle required for the identification of the grains based on EBSD was defined as 15° so that all boundary segments with an angle higher than 15° were considered to be grain boundaries. The grain orientation spread (GOS) map, which is widely used for the recrystallization analysis, was used to classify the grains having a GOS value of less than 2° into the recrystallized grains and to calculate the recrystallization fraction using the area fraction on the GOS map.

3.2.3 Computational details

It is possible to predict the recrystallization kinetics based on JMAK transformation kinetics (In chapter 2). However, this equation is only applicable to isothermal process. In a pulsed current treatment where the temperature changes continuously, is difficult to apply this equation as it is. Therefore, the equation was modified in conjunction with the rule of additivity for anisothermal process. The generalized form of the equation to predict the recrystallization fraction during continuous annealing can be expressed as [44]:

$$X_V = 1 - exp\left(-\left[\sum_{i=1}^{s}\left\{\int_{T_{i-1}}^{T_i}\frac{k(T)^{1/n}}{\gamma_i}dT + \left(\int k(T)^{1/n}dt\right)_{T_i}\right\}\right]^n\right) \quad (3.1)$$

where X_V is the volume fraction transformed, s is the number of annealing stages, γ_i is the rate of temperature change (positive for heating and negative for cooling) of the anisothermal stage, n is the Avrami exponent, and $k(T)$ is a term incorporating both the nucleation and growth rate of grains. In this study, since there is no isothermal stage during the processes, the isothermal holding time interval, dt, is zero and thus $\int k(T)^{1/n}dt$ at temperature T_i in Eq. (3.1) is also equal to zero.

By employing $k(T) = Aexp(-Q/RT)$, where A is a pre-exponential factor, Q is apparent activation energy, and R is the gas constant, Eq. (3.1) can be rewritten as:

$$X_V = 1 - exp\left[-A\left\{\sum_{i=1}^{s}\int_{T_{i-1}}^{T_i}\frac{\left(exp(-Q/RT)\right)^{1/n}}{\gamma_i}dT\right\}^n\right] \quad (3.2)$$

Equation (3.2) was used in this study to predict the recrystallization kinetic during the EPT. The variables s, T_{i-1}, T_i, and γ_i are input data obtained from the temperature histories measured (Figs. 3.3 and 3.4), and the parameters A, Q, and n can be determined through optimization based on GA and the method of least squares using commercial software MATLAB.

3.3 Analysis of recrystallization fraction by EPT

The EBSD inverse pole figure ND maps and GOS maps of the SPTed specimens according to current densities at 760℃ as a representative are shown in Fig. 3.5. The recrystallized grains are marked with blue color in the GOS map. The initial microstructure was measured to rarely have recrystallized grains as shown in Fig. 3.5 (a). Figures 3.5 (b)-(f) show that the recrystallized grains and deformed grains are mixed at all current density conditions. Among them, the specimen subjected to SPT with a current density of 68 A/mm^2 had the least recrystallized grains as depicted in GOS map of Fig. 3.5 (d). The microstructures of the SPTed specimens at different temperature conditions were also obtained in the same way. Based on EBSD GOS map analysis, the recrystallization fractions of all SPTed specimens are shown in Fig. 3.6. First, almost no recrystallization occurred regardless of the current density at peak temperature of 700℃. In contrast, at peak temperature of 860℃, recrystallization was almost completely finished under all current density conditions. However, at peak temperatures of 760℃ and 800℃, the amount of recrystallization fraction was appeared to be affected by current density. In both conditions, the smallest recrystallization fraction was observed at current density of 68 A/mm^2. As the current density increased or decreased based on 68 A/mm^2, the recrystallization fraction increased.

Vickers hardness was measured for 760℃ and 800℃ conditions and the result is shown in Fig. 3.7. The graph shape is the opposite of the recrystallization fraction analysis. The hardness was the highest at 68 A/mm^2, which was analyzed

to be the least recrystallized in GOS analysis. This is consistent with GOS analysis because the hardness decreases when recrystallization of dislocation-rich grain occurs. In other words, the hardness measurement confirms that the results of recrystallization fraction from EBSD GOS map analysis is reliable. In addition, because of the small deviation in hardness, it can be said that recrystallization occurred evenly throughout the specimen.

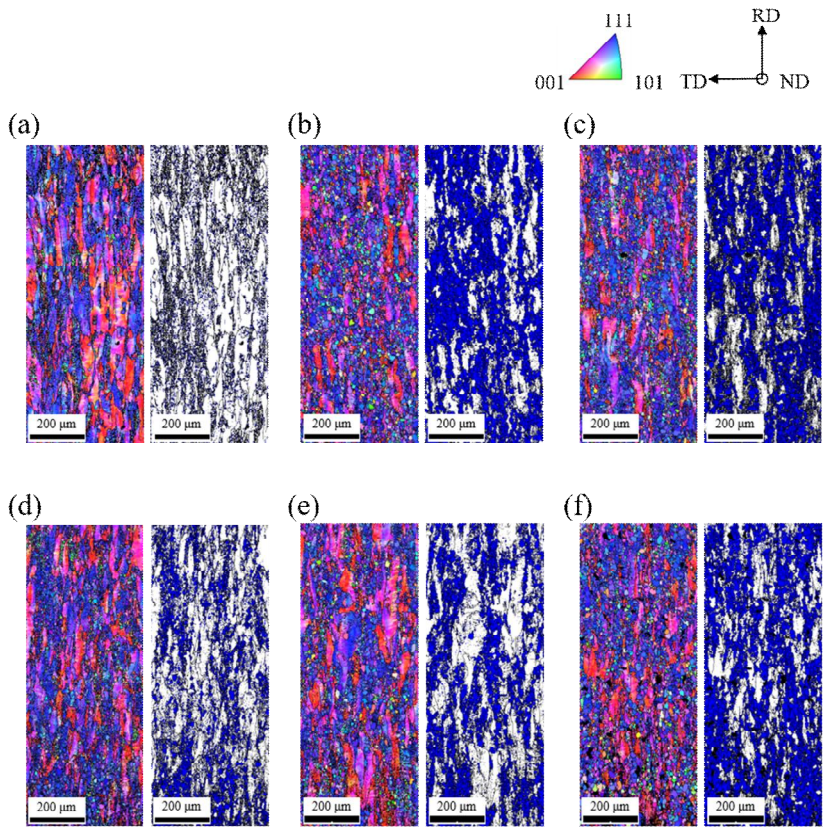

Figure 3.5 EBSD IPF maps and GOS maps of SPTed specimens with the current density of (a) 0 (initial), (b) 40, (c) 50, (d) 68, (e) 140 and (f) 210 Amm^2

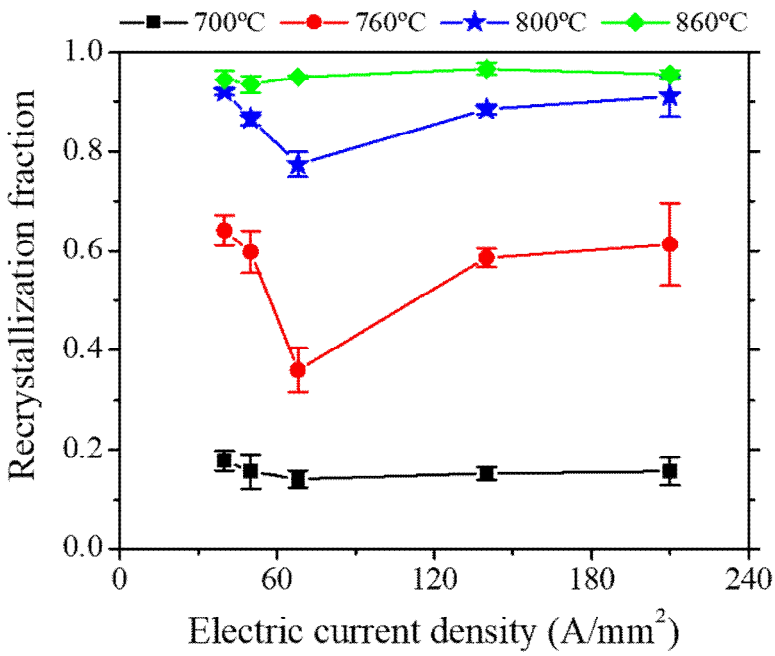

Figure 3.6 Recrystallization fractions of SPTed specimens with current density for the peak temperature of 700, 760, 800 and 860℃

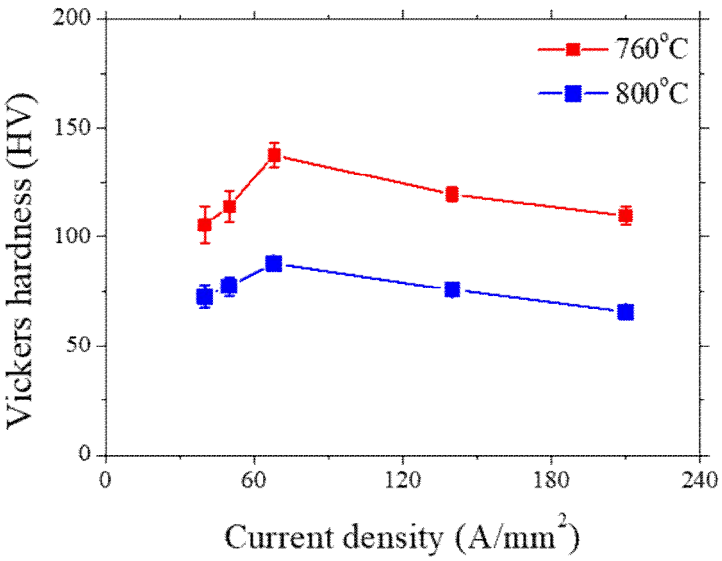

Figure 3.7 Vickers hardness results for the SPTed specimens with current density for the peak temperatures of 760 and 800℃

3.4 Analysis of recrystallization kinetic

Recrystallization fractions were analyzed on the CFTed specimens to confirm that Eq. (3.2) can accurately analyze the recrystallization kinetic. The recrystallization fraction through EBSD GOS analysis on CFTed specimens (Fig. 3.8) for four peak temperature conditions are shown in Fig 3.8. GA optimization was performed so that the recrystallization fraction calculated by Eq. (3.2) was similar to the recrystallization fraction obtained from the experiment (Fig. 3.9). Since the starting temperature of the recrystallization is higher than 500℃ in the case of ultra-low carbon steels [45-47], it is reasonable to calculate the recrystallization fraction using Eq. (3.2) by applying the initial temperature of 200℃, which is an experimentally measurable minimum value. At this time, The determined parameters are Q = 258.64 kJ/mol, n = 0.87 and A = 8.65 x 10^{11} s^{-1}, respectively. Since the recrystallization activation energy for cold-rolled steel is known to be about 150 to 400 kJ/mol [48, 49], and the average value of the Avrami exponent has been found close to 1 in other alloy systems [50], the obtained parameter values are reasonable. In this result, Eq. (3.2) can accurately calculate the recrystallization kinetic in the heat treatment.

In the SPT, the recrystallization kinetic on the temperature histories of peak temperature of 760 and 800℃ was predicted using Eq. (2) with determined parameters under calculation of CFT in Fig. 3.3 (Fig 3.10). It was predicted that recrystallization would occur less than 20% at both 760 and 800℃.

Recrystallization hardly occurs due to thermal effect by Joule heating of temperature history under SPT. These values all are markedly smaller than the actual measured values. This result clearly indicates that there is the athermal effect to recrysatllization when the electric current is applied.

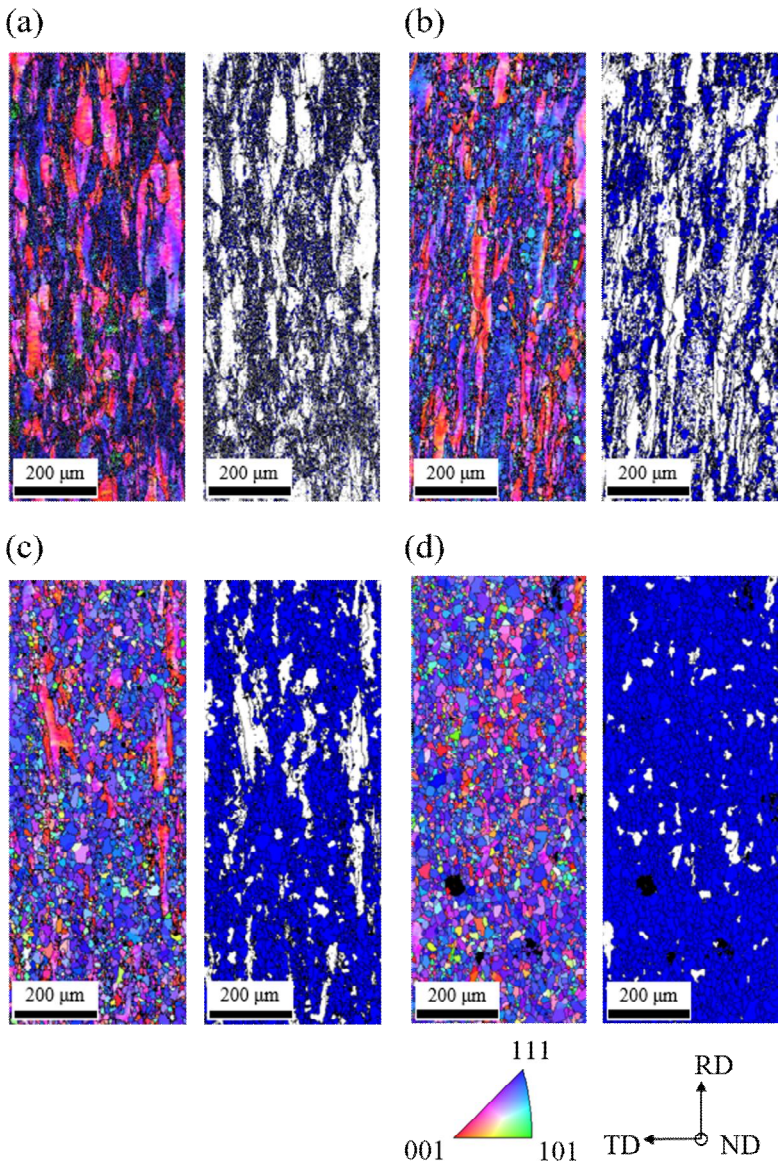

Figure 3.8 EBSD IPF maps and GOS maps of the CFTed specimens for the peak temperature of (a) 800, (b) 850, (c) 870 and (d) 900℃

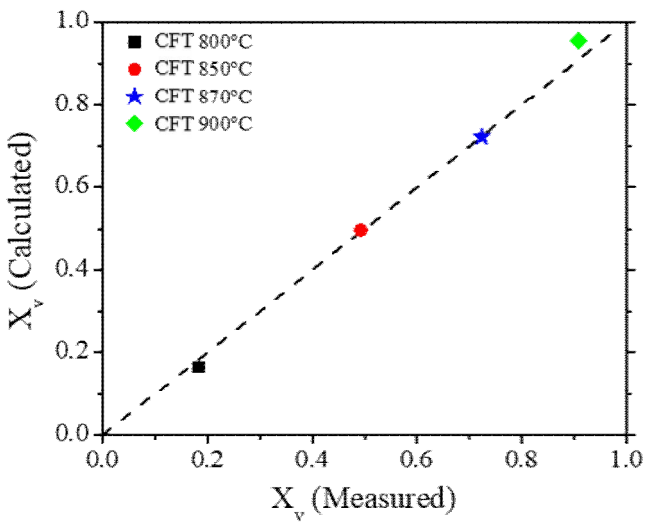

Figure 3.9 Comparison between measured recrystallization fractions and calculated recrystallization fractions using Eq. (3.2) of the CFTed specimens

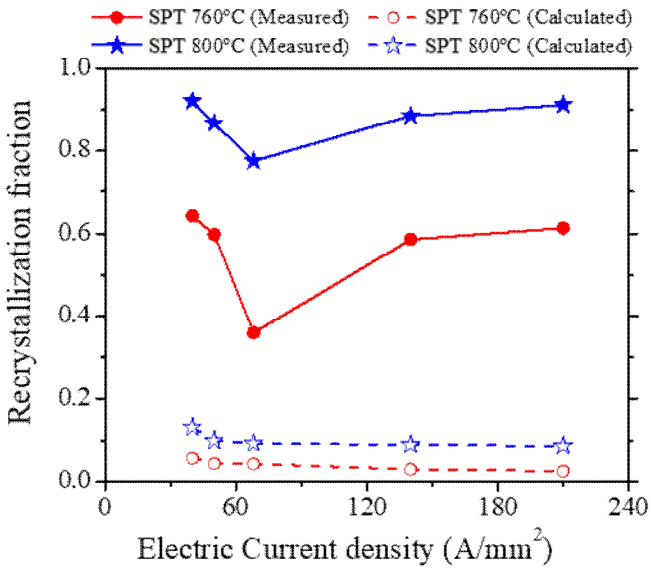

Figure 3.10 Comparison between measured recrystallization and recrystallization fractions predicted by Eq. (3.2) of the SPTed specimens for the peak temperatures of 760 and 800℃

3.5 Athermal effect of electric current-induced recrystallization

Reduction of activation energy barrier has been suggested in the earlier study to account for the athermal effect of the electric current in the recrystallization kinetic in Ch. 2. Based on this previous work, we investigated how electric current affected the athermal effect on recrystallization. First, it was thought that the electric current reduced the recrystallization activation energy in Ch. 2 (Fig. 3.11 (a)). The reduction of recrystallization activation energy was assumed to have a certain value depending on the current density. The athermal effect was considered to exist only during the electric current is applied. Thus, the Q_{eff} term was added to the section where electric current was applied, as described in Eq. (3.3)

$$X_V = 1 - exp\left[-A\left\{\sum_{i=1}^{p}\int_{T_{i-1}}^{T_i}\frac{\left(exp(-(Q-Q_{eff})/RT)\right)^{1/n}}{\gamma_i}dT + \sum_{i=p}^{f-1}\int_{T_i}^{T_{i+1}}\frac{\left(exp(-Q/RT)\right)^{1/n}}{\gamma_{i+1}}dT\right\}^{n}\right] \quad (3.3)$$

where p and f indicate the peak and the final points, respectively. Figure 3.11 (b) shows the results of the calculated recrystallization fractions with respect to the current densities of the SPTed specimens of the peak temperature of 760 and 800℃ through Eq. (3.3). The recrystallization fractions calculated with considering the reduction of recrystallization activation energy show V-shape curves as the current density increases, which are in good agreement with the measured results. Thus, it

can be seen empirically that the electric current affects the recrystallization activation energy term.

As mentioned in the Introduction (Ch.1) above, if the bonding energy of the atom near the grain boundary was weakened by the electric current, it may be considered that the phonon increased. As the temperature inside the material increases, the phonon energy increases. In other words, the temperature does not actually increase when the electric current is applied, but it can be assumed that the atoms behave as if the temperature rose as shown in Fig. 3.12 (a). In other words, effective temperature increased. Therefore, the T_{eff} term was added to the section where electric current was applied, the expression is as follows.

$$X_V = 1 - exp\left[-A\left\{\sum_{i=1}^{p}\int_{T_{i-1}}^{T_i}\frac{\left(exp\left(-Q/R(T+T_{eff})\right)\right)^{1/n}}{\gamma_i}dT + \sum_{i=p}^{f-1}\int_{T_i}^{T_{i+1}}\frac{\left(exp(-Q/RT)\right)^{1/n}}{\gamma_{i+1}}dT\right\}^{n}\right] \quad (3.4)$$

Similarly, the recrystallization fractions were predicted for SPT at 760 and 800℃ (Fig. 3.12 (b)). The recrystallization fractions calculated by considering the increase of effective temperatures show V-shape curves as the current density increases, which are in good agreement with the measured results. Therefore, the athermal effect is also described to the effective temperature.

The predicted amounts of effective activation energy reduction (blue) and effective temperature increase (red) depending on the current density are shown in Fig. 3.13. As the current density increases, a reasonable tendency is observed in

which the amount of recrystallization activation energy is reduced or effective temperature is increased. Moreover, by plotting graphs that fit well with these data, we can establish relationship that the effective amounts of activation energy and temperature are approximately proportional to the square root of the current density as shown in Eqs. (3.5) and (3.6).

$$\Delta G = 4.96\sqrt{j} \tag{3.5}$$

$$\Delta T = 22.82\sqrt{j} \tag{3.6}$$

Therefore, we can explicate the athermal effect as weakened bonding strength between atoms appears as the effective reduction of the activation energy or the effective increase of temperature clearly distinct from conventional Joule heating in the case of recrystallization by the SPT.

Based on this study, we expect that the optimal SPT processing condition to maximize the athermal effect can be designed, which will contribute to enhance the mechanical properties of the materials as well as the efficiency of the SPT process.

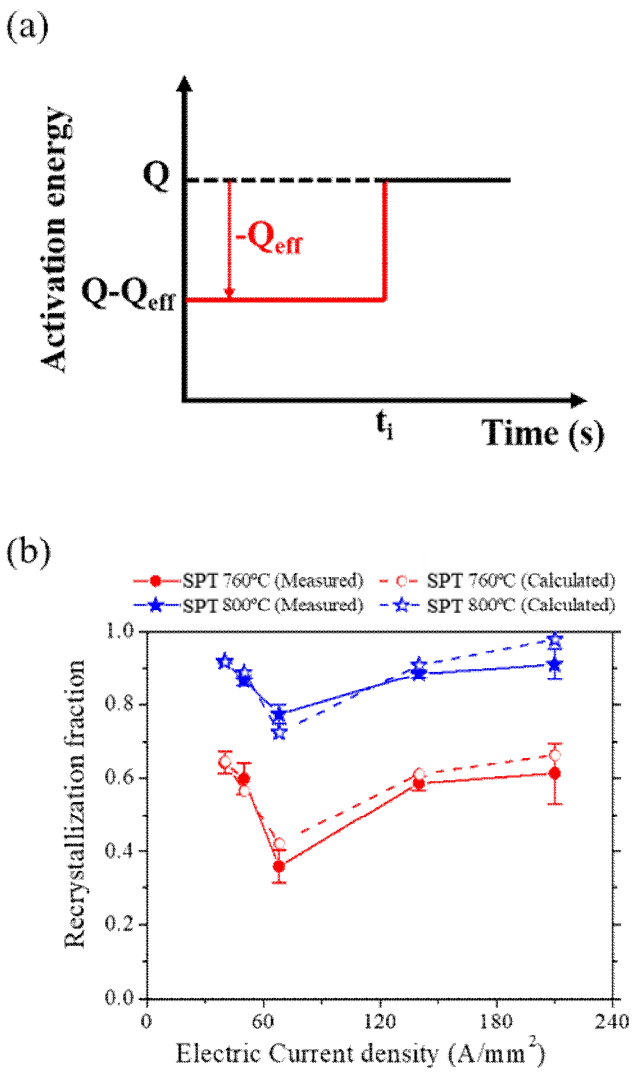

Figure 3.11 (a) Schematic for the concept of the reduction of recrystallization activation energy, and (b) comparison of recrystallization fractions calculated using Eq. (3) and measured values

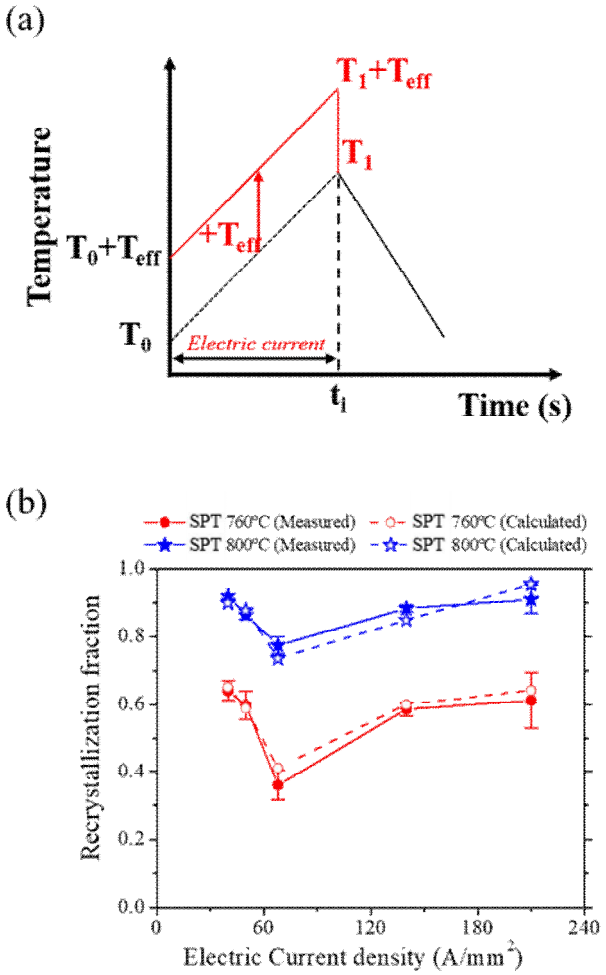

Figure 3.12 (a) Schematic for the concept of the increase of effective temperature, and (b) comparison of recrystallization fractions calculated using Eq. (3.3) and measured values

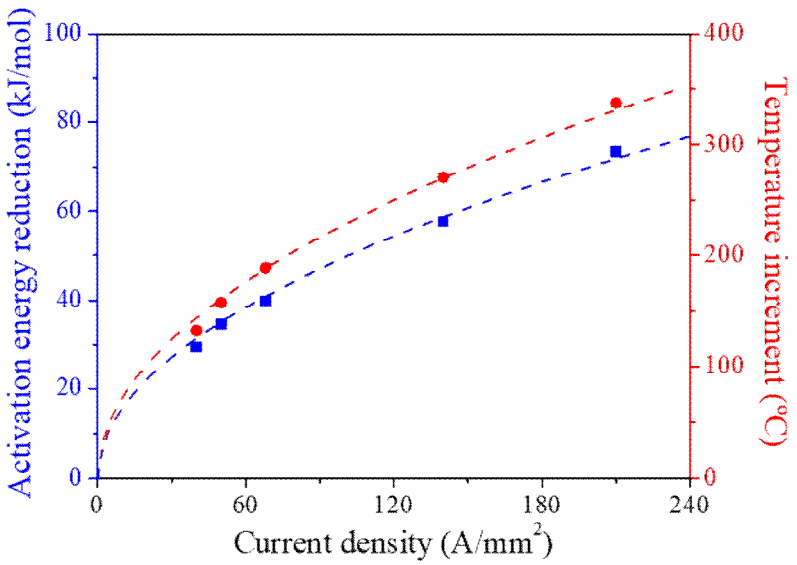

Fig. 3.13 Amount of the effective activation energy reduction (blue) and temperature increment (red) with five different current densities, and fitted graphs (dash lines)

3.6 Conclusion

To investigate and quantify the effect of the electric current on annealing of ultra-low carbon steel, a single pulse of electric current is applied to the specimens under five different current densities with duration times adjusted to reach the target annealing temperatures. As a result of the microstructure analysis of the specimens subjected to the SPT so that the peak annealing temperatures are 760 and 800℃, recrystallization fraction tend to decrease as the current density increases up to 68 A/mm^2, while they tend to increase under higher current densities than 68 A/mm^2. Vickers hardness results support the tendency of recrystallization over the current density. Through comparison with the CFT, it is confirmed that the recrystallization can occur at lower temperature under the SPT than under HT due to athermal effect of electric current. In addition, the athermal effect also can be demonstrated and quantified by comparing the recrystallization fraction measured by the SPT experiment with the calculated one using the modified JMAK equation adopting the additivity rule. It is shown that the athermal effect, which is distinct from the thermal effect due to conventional Joule heating, can be described by introducing the concept of the reduction of recrystallization activation energy or the effective temperature increase. Based on these concepts, we can find that the amount of recrystallization activation energy reduction or effective temperature increase is proportional to the square root of the current density.

3.7 Reference

[1] I. Khaibullin, E. Shtyrkov, M. Zaripov, R. Bayazitov, M. Galjautdinov, Some features of laser annealing of implanted silicon layers, Radiat. EIT. 36(3-4) (1978) 225-233.

[2] R.E. Haimbaugh, Practical induction heat treating, ASM international 2001.

[3] H. Conrad, N. Karam, S. Mannan, Effect of electric current pulses on the recrystallization of copper, Scr. Metall. 17(3) (1983) 411-416.

[4] H. Conrad, N. Karam, S. Mannan, A. Sprecher, Effect of electric current pulses on the recrystallization kinetics of copper, Scr. Metall. 22(2) (1988) 235-238.

[5] K. Huang, C. Cayron, R.E. Logé, The surprising influence of continuous alternating electric current on recrystallization behaviour of a cold-rolled Aluminium alloy, Mater. Charact. 129 (2017) 121-126.

[6] Z.S. Xu, Y.X. Chen, Effect of electric current on the recrystallization behavior of cold worked α-Ti, Scr. Metall. 22(2) (1988) 187-190.

[7] E.S. Machlin, Applied voltage and the plastic properties of``Brittle"rock salt, J. Appl. Phys. 30(7) (1959) 1109-1110.

[8] H. Conrad, Electroplasticity in metals and ceramics, Mater. Sci. Eng., A 287(2) (2000) 276-287.

[9] M.-J. Kim, K. Lee, K.H. Oh, I.-S. Choi, H.-H. Yu, S.-T. Hong, H.N. Han, Electric current-induced annealing during uniaxial tension of aluminum alloy, Scr. Mater. 75 (2014) 58-61.

[10] J.T. Roth, I. Loker, D. Mauck, M. Warner, S.F. Golovashchenko, A. Krause, Enhanced formability of 5754 aluminum sheet metal using electric pulsing,

Transactions of the North American Manufacturing Research Institution of SME, 2008, pp. 405-412.

[11] W.A. Salandro, J.J. Jones, C. Bunget, L. Mears, J.T. Roth, Introduction to electrically assisted forming, Electrically Assisted Forming, Springer 2015, pp. 23-36.

[12] O. Troitskii, Electromechanical effect in metals, ZhETF Pisma Redaktsiiu 10 (1969) 18.

[13] N. Bertolino, J. Garay, U. Anselmi-Tamburini, Z. Munir, High-flux current effects in interfacial reactions in Au–Al multilayers, Philos. Mag. B 82(8) (2002) 969-985.

[14] S.-W. Chen, C.-M. Chen, W.-C. Liu, Electric current effects upon the Sn/Cu and Sn/Ni interfacial reactions, J. Electron. Mater. 27(11) (1998) 1193-1199.

[15] H.-J. Jeong, M.-J. Kim, J.-W. Park, C.D. Yim, J.J. Kim, O.D. Kwon, P.P. Madakashira, H.N. Han, Effect of pulsed electric current on dissolution of Mg17Al12 phases in as-extruded AZ91 magnesium alloy, Mater. Sci. Eng., A 684 (2017) 668-676.

[16] T. Wang, J. Xu, T. Xiao, H. Xie, J. Li, T. Li, Z. Cao, Evolution of dendrite morphology of a binary alloy under an applied electric current: An in situ observation, Phys. Rev. E 81(4) (2010) 042601.

[17] M.-J. Kim, H.-J. Jeong, J.-W. Park, S.-T. Hong, H.N. Han, Modified Johnson-Cook model incorporated with electroplasticity for uniaxial tension under a pulsed electric current, Met. Mater. Int. 24(1) (2018) 42-50.

[18] G. Hu, G. Tang, Y. Zhu, C. Shek, Electropulsing induced texture evolution in the recrystallization of Fe-3 Pct Si alloy strip, Metall. Mater. Trans. A 42(11) (2011) 3484.

[19] R. Qin, A. Rahnama, W. Lu, X. Zhang, B. Elliott-Bowman, Electropulsed steels, Mater. Sci. Technol. 30(9) (2014) 1040-1044.

[20] Y. Zhou, J. Guo, W. Zhang, G. He, Influence of electropulsing on nucleation during phase transformation, J. Mater. Res. 17(12) (2002) 3012-3014.

[21] Y. Zhou, W. Zhang, B. Wang, J. Guo, Ultrafine-grained microstructure in a Cu–Zn alloy produced by electropulsing treatment, J. Mater. Res. 18(8) (2003) 1991-1997.

[22] R. Fan, J. Magargee, P. Hu, J. Cao, Influence of grain size and grain boundaries on the thermal and mechanical behavior of 70/30 brass under electrically-assisted deformation, Mater. Sci. Eng., A 574 (2013) 218-225.

[23] J. Magargee, R. Fan, J. Cao, Analysis and observations of current density sensitivity and thermally activated mechanical behavior in electrically-assisted deformation, J. Manuf. Sci. Eng. 135(6) (2013) 061022.

[24] D. Ben, H. Yang, Y. Ma, X. Shao, J. Pang, Z. Zhang, Rapid hardening of AISI 4340 steel induced by electropulsing treatment, Mater. Sci. Eng., A 725 (2018) 28-32.

[25] Y. Ma, H. Yang, Y. Tian, J. Pang, Z. Zhang, Hardening and softening mechanisms in a nano-lamellar austenitic steel induced by electropulsing treatment, Mater. Sci. Eng., A 713 (2018) 146-150.

[26] C. Li, S. Jiang, K. Zhang, Pulse current-assisted hot-forming of light metal alloy, Int. J. Adv. Manuf. Technol. 63(9-12) (2012) 931-938.

[27] J. Magargee, F. Morestin, J. Cao, Characterization of flow stress for commercially pure titanium subjected to electrically assisted deformation, J. Eng. Mater. Technol. 135(4) (2013) 041003.

[28] A. Rahnama, R. Qin, Room temperature texturing of austenite/ferrite steel by electropulsing, Sci. Rep. 7 (2017) 42732.

[29] D. Xu, B. Lu, T. Cao, H. Zhang, J. Chen, H. Long, J. Cao, Enhancement of process capabilities in electrically-assisted double sided incremental forming, Mater. Des. 92 (2016) 268-280.

[30] J.-H. Roh, J.-J. Seo, S.-T. Hong, M.-J. Kim, H.N. Han, J.T. Roth, The mechanical behavior of 5052-H32 aluminum alloys under a pulsed electric current, Int. J. Plast. 58 (2014) 84-99.

[31] J.-W. Park, H.-J. Jeong, S.-W. Jin, M.-J. Kim, K. Lee, J.J. Kim, S.-T. Hong, H.N. Han, Effect of electric current on recrystallization kinetics in interstitial free steel and AZ31 magnesium alloy, Mater. Charact. 133 (2017) 70-76.

[32] S. Lin, X. Chu, W. Bao, J. Gao, L. Ruan, Experimental investigation of pulse current on mechanical behaviour of AZ31 alloy, Mater. Sci. Technol. 31(9) (2015) 1131-1138.

[33] M.-J. Kim, M.-G. Lee, K. Hariharan, S.-T. Hong, I.-S. Choi, D. Kim, K.H. Oh, H.N. Han, Electric current–assisted deformation behavior of Al-Mg-Si alloy under uniaxial tension, Int. J. Plast. 94 (2017) 148-170.

[34] C.D. Ross, D.B. Irvin, J.T. Roth, Manufacturing aspects relating to the effects of direct current on the tensile properties of metals, J. Eng. Mater. Technol. 129(2) (2007) 342-347.

[35] Y.Z. Zhou, W. Zhang, J. Guo, G. He, Diffusive phase transformation in a Cu–Zn alloy under rapid heating by electropulsing, Philos. Mag. Lett. 84(5) (2004) 341-348.

[36] Y.J. Lee, H.-M. Sung, Y. Jin, K. Lee, C.R. Park, G.-H. Kim, H.N. Han, Improvement of mechanical property of air plasma sprayed tungsten film using

pulsed electric current treatment, Int. J. Refract. Met. Hard Mater. 60 (2016) 99-103.

[37] H. Conrad, Thermally activated plastic flow of metals and ceramics with an electric field or current, Mater. Sci. Eng., A 322(1-2) (2002) 100-107.

[38] O. Troitskii, V. Likhtman, The Effect of the Anisotropy of Electron and Radiation on the Deformation of zinc single crystals in the Brittle State, Akaciemiya Nauk SSSR 147(4) (1963) 814-820.

[39] A. Sprecher, S. Mannan, H. Conrad, Overview no. 49: On the mechanisms for the electroplastic effect in metals, Acta Metall. 34(7) (1986) 1145-1162.

[40] X.-P. Lu, W.-D. Cao, A. Sprecher, H. Conrad, Influence of an external electric field on the microstructure of superplastically deformed 7475 Al, J. Mater. Sci. 27(8) (1992) 2243-2250.

[41] H. Conrad, W. Cao, X. Lu, A. Sprecher, Effect of an electric field on the superplasticity of 7475 Al, Scr. Metall. 23(5) (1989) 697-702.

[42] K. Okazaki, M. Kagawa, H. Conrad, An evaluation of the contributions of skin, pinch and heating effects to the electroplastic effect in titatnium, Mater. Sci. Eng., A 45(2) (1980) 109-116.

[43] M. Molotskii, V. Fleurov, Magnetic effects in electroplasticity of metals, Phys. Rev. B 52(22) (1995) 15829.

[44] M. Ferry, D. Muljono, D. DP, Recrystallization kinetics of low and ultra low carbon steels during high-rate annealing, ISIJ Int. 41(9) (2001) 1053-1060.

[45] E. Novillo, M.M. Petite, J.L. Bocos, A. Iza□Mendia, I. Gutiérrez, Texture and Microtexture Evolution in an Ultra□Low Carbon Steel During Recrystallization, Adv. Eng. Mater. 5(8) (2003) 575-578.

[46] H.N. Han, J.K. Lee, S.-J. Kim, An observation of permanent strain during recrystallization and growth of steel under externally applied stress, Mater. Lett. 59(2-3) (2005) 158-161.

[47] F. Castro Cerda, L. Kestens, A. Monsalve, R. Petrov, The effect of ultrafast heating in cold-rolled low carbon steel: Recrystallization and texture evolution, Metals 6(11) (2016) 288.

[48] W. Bleck, R. Bode, F.-J. Hahn, Production and Properties of IF(Interstitial-Free) Steel, Thyssen Tech. Ber. 22(1) (1990) 69-85.

[49] C. Huang, E. Hawbolt, X. Chen, T. Meadowcroft, D. Matlock, Flow stress modeling and warm rolling simulation behavior of two Ti–Nb interstitial-free steels in the ferrite region, Acta Mater. 49(8) (2001) 1445-1452.

[50] F.J. Humphreys, M. Hatherly, Recrystallization and related annealing phenomena, Elsevier 2012.

Chapter 4

Investigation of athermal effect of electric current in electroplasticity

4.1 Introduction

Microstructural change of a conductive metallic materials can be accelerated by applying electric current [17,18]. Electropulsing treatment (EPT) is an effective technique that changes the microstructure of a metallic material and improves its physical properties by applying high electric current density at relatively low temperature [19]. The theoretical background of EPT could be described from some studies on thermal and athermal effects of electric current. In 1959, Machlin [20] reported that electric pulsing can significantly affect the plastic properties of a brittle rock salt. Thereafter, it has been reported that the mechanical behavior of various materials may be affected by applying high current density during deformation [21-29]. Moreover, many studies have reported that the changes in the microstructure of materials are able to be controlled and accelerated by applying electric current with high current density to the material without deformation [30-37]. Conrad et al. [30,31] reported that the electric current itself could have an effect on the recrystallization kinetic of pure copper in addition to the well-known thermal effect by Joule heating. Wang et al. [32] stated that electric current can

affect dendritic growth during the solidification of Sn/Pb binary alloys. Recently, it was reported that the dissolution of intermetallic compounds in AZ91 magnesium alloy was accelerated by applying pulsed electric current [33]. It was also reported that sintering of tungsten was carried out by EPT to accelerate densification and improve mechanical properties even at a lower temperature than the temperature of conventional pressurized heat treatment [34].

In Ch. 3, the athermal effect of electric current was discussed in terms of the concept of reduction of recrystallization activation energy and effective temperature. Among these concepts, we checked whether the effective temperature could be applied to the electroplasticity. The tensile behavior of pulsed tensile test was analyzed by FE constitutive calculation for low carbon steel.

4.2 Experimental procedure

4.2.1 Material and instrumental set-up

A commercial EDDQ grade (Fe-0.005C-0.01Si-0.05Mn-0.004P-0.005S-0.005Ni-0.0Cr-0.001Mo in wt%) steel sheet was used in this study. It was fully annealed state. Microstructure of as-received specimen is showed in Fig. 4.1.

The uniaxial tensile test was conducted at the constant crosshead speed of 1.0 mm/min. Fig. 4.2 shows the instrumental set-up for pulsed tensile test. Two tensile test machine was used. For pulsed tensile test, INSTRON 5584 (INSTRON, USA) which is modified to can apply electric current to the specimen was used. Bakelite was inserted between the specimen and each grip to prevent leakage of electric current into the equipment. For high temperature tensile test, INSTRON 5582 (INSTRON, USA) which has additional furnace was used. The specimens for the tensile test were processed to the ASTM E8 subsize with a gauge width of 6.25 mm and a gauge length of 25 mm along the rolling direction. The strain was measured by ARAMIS digital image correlation (DIC) (GOM, Germany), which can measure relative displacements of characteristic points on the digital images. For DIC strain measurement, a black small dot random pattern was formed using spray paint to create a high contrast with the white surface coating and displacement measurement was taken from this surface pattern.

For the pulsed tensile test, the electric current was applied by a Vadal SP-1000U DC power supply (Hyosung, South Korea) and periodically applied to the specimen with a duration (t_d) of 0.1 sec and a period (t_p) of 40 sec during uniaxial

tensile test. The current density was 105 A/mm^2 based on the initial cross-sectional area of the specimen. The first pulse was applied above 200 MPa.

Temperature during pulsed tensile test was measured by a FLIR-T430 infra-red (IR) thermal imaging camera (FLIR, Sweden). For this measurement, high temperature black paint was sprayed to the opposite side of the strain measurement side to fix the emissivity of the specimen. An emissivity of 0.95 was used after calibration with the black spray. Temperature during heat treated tensile test was measured by K-type thermocouple. The thermocouple was attached to the center of the specimen.

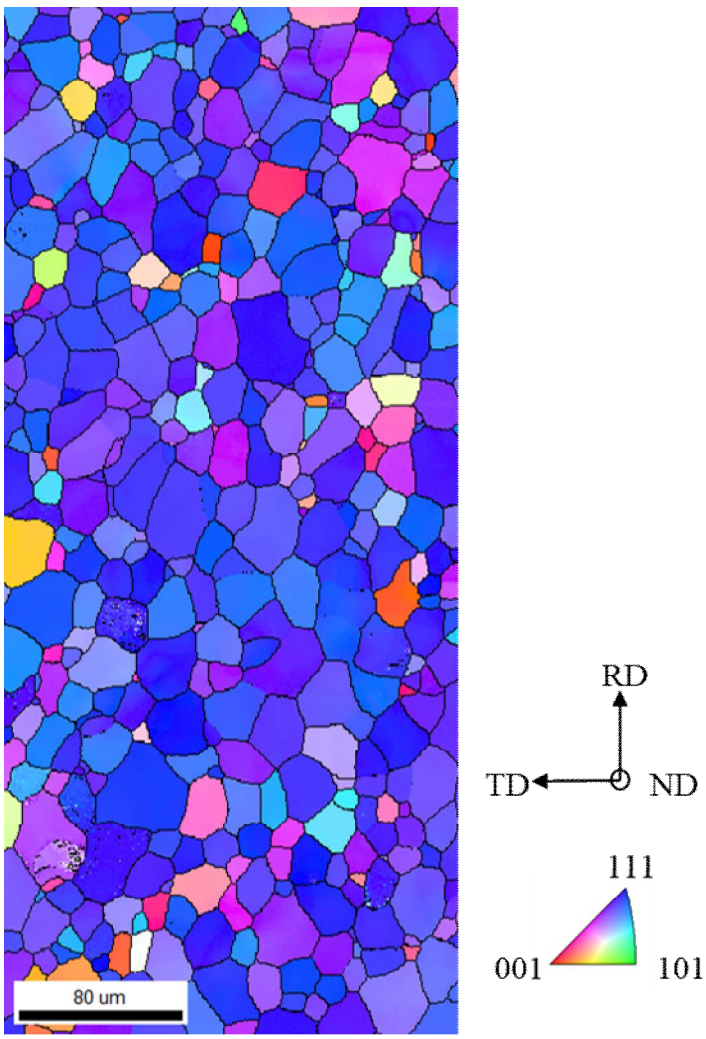

Figure 4.1 EBSD IPF ND map of as-received specimen

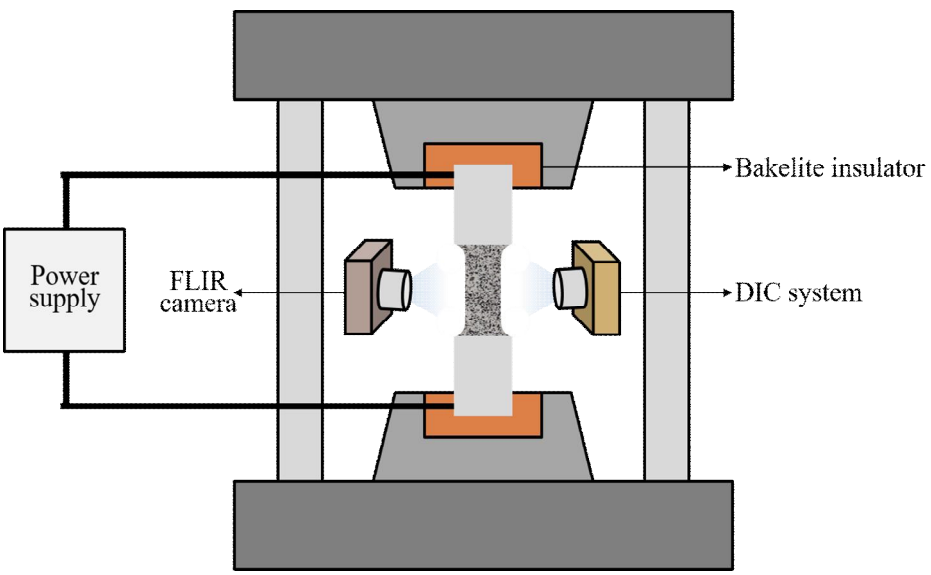

Figure 4.2 Instrumental set-up for pulsed tensile test

4.2.2 Computational details

FE analysis of uniaxial tensile test under electric current was carried out considering effective temperature suggested in the main text. Three dimensional FE mesh was constructed from EBSD image of initial microstructure (Fig. 4.3). The model dimension was 72 μm × 74 μm × 1 μm with element size of 0.5^{-1} μm. The number of elements and nodes were 6844 and 13984 respectively. Thermal expansion coefficient and density were 11.7 μm/m·℃ and 7.86 kg/m^3, respectively. The calculation based on the actual microstructure caused a problem that the temperature of the grain boundary could not be set high. Grain boundary length was calculated from the area of the constructed model and was 982 μm. Therefore, the model was reconstructed in a simple form while maintaining the ratio of grain boundaries to the whole area.

The hardening model used in the present study assumed that the strain hardening during uniaxial tension is mostly from dislocation-dislocation interactions [18, 19]. This assumption holds true when the grain size is relatively large and other hardening mechanisms are insignificant. The flow stress σ can be described as a function of dislocation density and strain rate as

$$\sigma = (\sigma_0 + \mathrm{M}\alpha\mathrm{Gb}\sqrt{\rho})\left(\frac{\dot{\varepsilon}}{\dot{\varepsilon_0}}\right)^{1/m} \quad (4.1)$$

where M, G, and b are Taylor factor, shear modulus, and burgers vector, respectively. σ_0, α, $\dot{\varepsilon_0}$, and m are material parameters. Here, the parameter σ_0 is considered as a function of temperature and is given by

$$\sigma_0 = A \cdot T^B + C \tag{4.2}$$

where A, B, and C are material constants. Similar to σ_0, α is proposed to be

$$\alpha = \lambda_1 \cdot T^{\lambda_2} + \lambda_3 \tag{4.3}$$

where λ_1, λ_2, and λ_3 are material constants. The evolution of dislocation density is given as

$$\frac{d\rho}{d\varepsilon} = \mathrm{M}\left(K_1\sqrt{\rho} - K_2\rho\right) \tag{4.4}$$

The parameters K_1 and K_2 are used to describe the behavior of formation and recovery of dislocation and K_2 is known as a function of temperature and strain rate [20]

$$K_2 = K_{20} \cdot \left(\frac{\dot{\varepsilon}}{\dot{\varepsilon}_0^*}\right)^{-1/n} \tag{4.5}$$

where K_{20}, $\dot{\varepsilon}_0^*$, and n are material constants. It is suggested that the parameter n is a function of temperature at low temperature region (typically T<0.5 T_m) and is given by

$$n = \xi_1 \cdot \left\{T^{\xi_2}\right\} \tag{4.6}$$

here ξ_1 and ξ_2 are material parameters. Through the FE analysis by hardening model, tensile behavior under electropulsed tensile test was predicted.

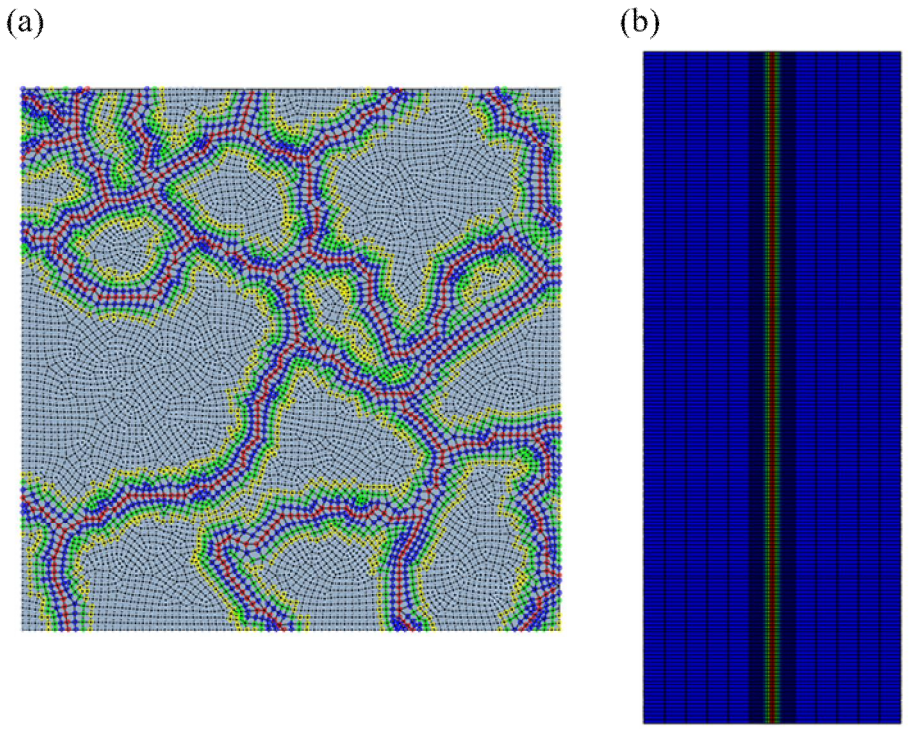

Figure 4.3 (a) Geometrical modeling of polycrystalline structure based on real microstructure for FE simulation of pulsed tensile test, and (b) simplified model taking into account the grain boundary length of (a)

4.3 Analysis of the electric current effect on the electroplasticity

Tensile tests were conducted at various temperatures to analyze the tensile behavior under pulsed tensile test and the results are shown in Fig. 4.4. The high temperature tensile test was performed at average temperatures of 80, 162 and 234℃. When the temperature at which the tensile test was conducted was increase, the ultimate tensile stress was decreased due to reduction of flow stress. However, the elongation decreased when the temperature increased.

FE analysis of high temperature tensile test was performed and the results are shown in Fig. 4.5. The parameters used in hardening model and the thermal properties are listed in Table. 4.1

The pulsed tensile test was performed and the result are shown in Fig. 4.6 (a). When the first pulse was applied, the temperature increased to 60℃. The peak temperature gradually increased as the number of pulses increased, and increased rapidly after necking. This is because the actual current density increased due to the decrease of the cross-sectional area as the tensile test proceeded. As soon as the electric pulse was applied, a large stress drop occurred. The stress at the first pulse dropped by 80 MPa. As the pulsed tension progressed, the flow stress gradually decreased. Like high temperature tensile test, the elongation was reduced compared to non-pulsed tensile test.

The result of the FE analysis using the parameters obtained from optimization

of high temperature tensile test using the temperature history of pulsed tension are shown in Fig. 4.7. stress drop of pulsed tensile test cannot be fully reproduced by the consideration of only both the thermal expansion and the decrease of elastic modulus due to spontaneous temperature increase.

In order to consider the athermal effect of electric current, we implemented the concept of effective temperature in the FE simulation for electroplastic deformation based on analysis result in Ch. 3. The effective temperatures rise was set as approximately 300℃ at center of grain boundary and 100℃ at side of grain boundary considering the atomic structure of grain boundary (Fig. 4.8). Therefore, the average effective temperature was set to about 200℃. The calculated electrically-assisted tensile behaviors considering the effective temperature are superimposed with experimental EA result in Fig. 4.9. Electroplastic deformation behavior under electric current is well described by the FE simulation incorporated with the concept of the effective temperature. Through this results, it was confirmed that the athermal effect of the electric current in the electroplasticity can be completely explained by the effective temperature concept.

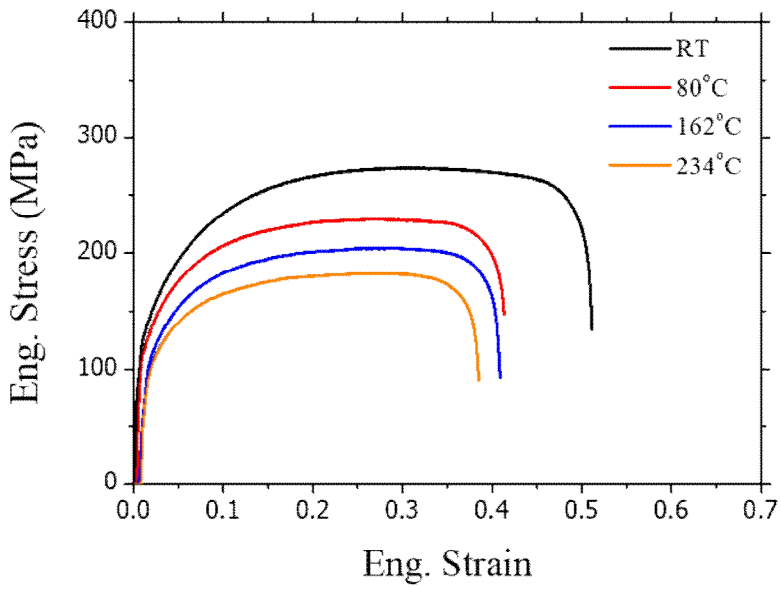

Figure. 4.4 Stress-strain curves at various temperatures

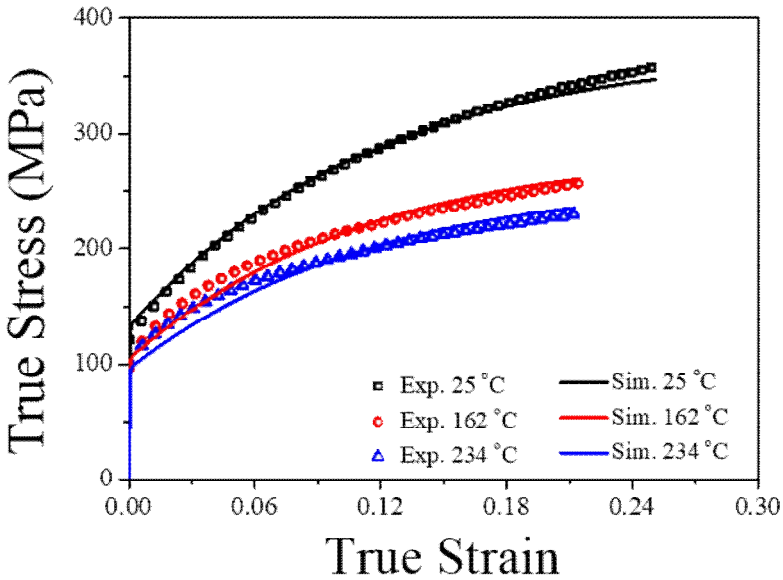

Figure 4.5 Comparison of simulation curves with the experimental curves of tensile test at high temperatures

Table. 4.1 Material parameters obtained from FE simulation of tensile test at high temperatures

M	α			G	b	σ_0	$\dot{\boldsymbol{\varepsilon}}_{\mathbf{0}}$
	λ_1	λ_2	λ_3	(GPa)	(m)	(MPa)	
2.71	4.26	4.26	-0.70	80	2.5×10^{-10}	15	3.24×10^{-6}

M	K_1	K_2			
		K_{20}	$\dot{\varepsilon}_0^*$	ξ_1	ξ_2
41.05	1.11×10^{8}	6.44	3.52×10^{-4}	0.8324	0.93

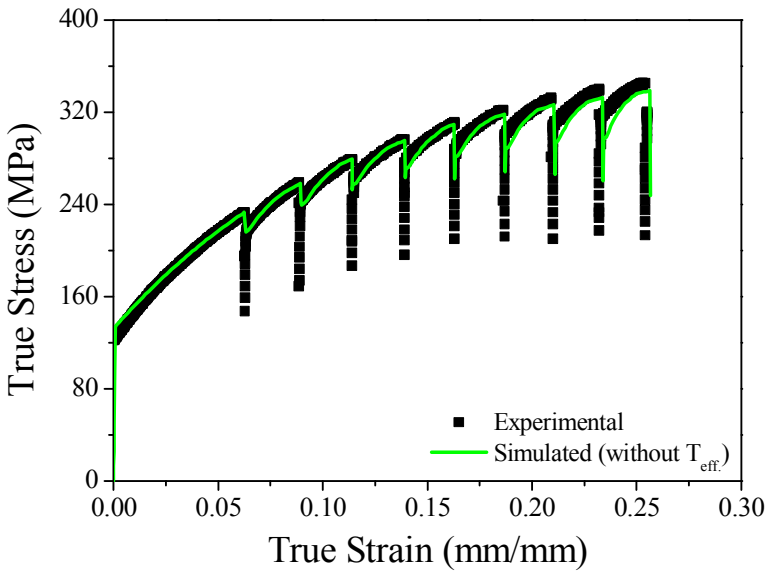

Figure 4.6 Comparison of simulation curves with the experimental curves of pulsed tensile test considering only temperature history

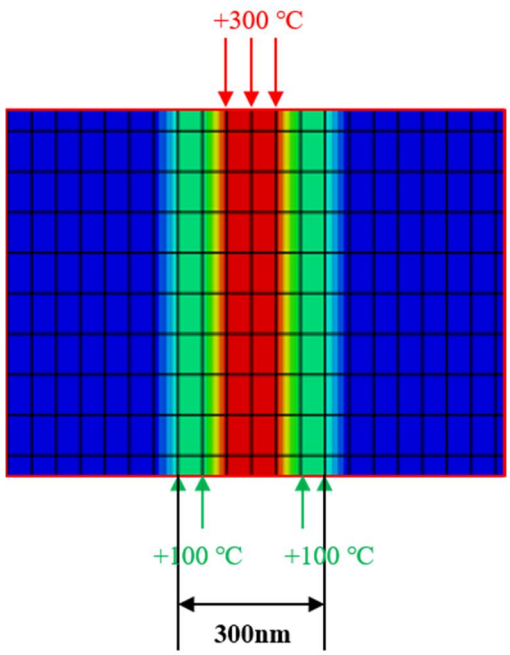

Figure 4.7 Effective temperature imposed on grain boundary

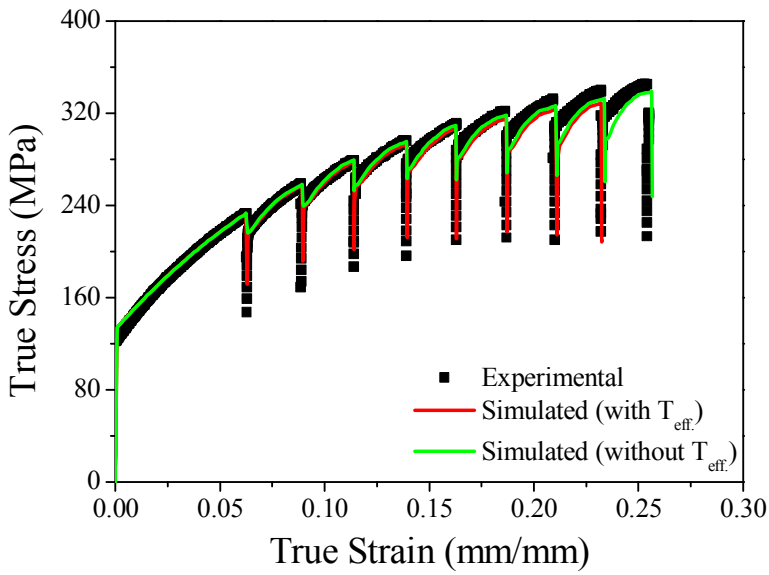

Figure 4.8 Comparison of simulation curves with the experimental curves of pulsed tensile test considering effective temperature

4.4 Conclusion

The present work demonstrates that the athermal effect of electric current is a result of additional weakening of atomic bonding strength around grain boundary. The additional weakening of atomic bonding strength under electric current can be described by introducing the concept of effective temperature, which is a sum of the virtual temperature increase by athermal effect of electric current and the physically measured temperature increase by Joule heating. Based on the FE constitutive analysis at high temperature tensile test, the result of pulsed tensile test was also analyzed. When interpreted only by the temperature history of pulsed tensile test, little stress drops were calculated compared with the experimental values. However, when the about 200℃ of effective temperature was imposed to the grain boundary, the stress drop could be completely explained. This value was similar compared to the effective temperature obtained in Ch. 3. Therefore, it can be confirmed again that the derived result of the effective temperature increase as a function of current density in Ch. 3 is reliable. In addition, atomic diffusion enhancement throughout EAM phenomena including electroplasticity and electropulsing treatment can be explained fully by the effective temperature.

4.5 References

[1] Guan, L., Tang, G., Jiang, Y., and Chu, P. K. (2009). Texture evolution in cold-rolled AZ31 magnesium alloy during electropulsing treatment. Journal of Alloys and Compounds, 487(1-2), 309-313.

[2] Konovalov, S., Atroshkina, A., Ivanov, Y. F., and Gromov, V. (2010). Evolution of dislocation substructures in fatigue loaded and failed stainless steel with the intermediate electropulsing treatment. Materials Science and Engineering: A, 527(12), 3040-3043.

[3] Lai, Z., Conrad, H., Chao, Y., Wang, S., and Sun, J. (1989). Effect of electropulsing on the microstructure and properties of iron-based amorphous alloys. Scripta metallurgica, 23(3), 305-310.

[4] Machlin, E. (1959). Applied voltage and the plastic properties of``Brittle''rock salt. Journal of applied physics, 30(7), 1109-1110.

[5] Fan, R., Magargee, J., Hu, P., and Cao, J. (2013). Influence of grain size and grain boundaries on the thermal and mechanical behavior of 70/30 brass under electrically-assisted deformation. Materials Science and Engineering: A, 574, 218-225.

[6] Kim, M.-J., Lee, M.-G., Hariharan, K., Hong, S.-T., Choi, I.-S., Kim, D. and Han, H. N. (2017). Electric current–assisted deformation behavior of Al-Mg-Si alloy under uniaxial tension. International Journal of Plasticity, 94, 148-170.

[7] Roh, J.-H., Seo, J.-J., Hong, S.-T., Kim, M.-J., Han, H. N. and Roth, J. T. (2014). The mechanical behavior of 5052-H32 aluminum alloys under a pulsed electric

current. International Journal of Plasticity, 58, 84-99.

[8] Kim, M. J., Lee, K., Oh, K. H., Choi, I. S., Yu, H. H., Hong, S. T. and Han, H. N. (2014). Electric current-induced annealing during uniaxial tension of aluminum alloy. Scripta Materialia, 75, 58-61, doi:10.1016/j.scriptamat.2013.11.019.

[9] Conrad, H. (2000). Electroplasticity in metals and ceramics. Materials Science and Engineering: A, 287(2), 276-287.

[10] Oh, H.-S., Cho, H.-R., Park, H., Hong, S.-T. and Chun, D.-M. (2016). Study of electrically-assisted indentation for surface texturing. International Journal of Precision Engineering and Manufacturing-Green Technology, 3(2), 161-165.

[11] Thien, N. T., Jeong, Y.-H., Hong, S.-T., Kim, M.-J., Han, H. N. and Lee, M.-G. (2016). Electrically assisted tensile behavior of complex phase ultra-high strength steel. International Journal of Precision Engineering and Manufacturing-Green Technology, 3(4), 325-333.

[12] Jeong, H.-J., Park, J.-w., Jeong, K. J., Hwang, N. M., Hong, S.-T. and Han, H. N. (2019). Effect of pulsed electric current on TRIP-aided steel. International Journal of Precision Engineering and Manufacturing-Green Technology, 6(2), 315-327.

[13] Kim, M.-J., Jeong, H.-J., Park, J.-W., Hong, S.-T. and Han, H. N. (2018). Modified Johnson-Cook model incorporated with electroplasticity for uniaxial tension under a pulsed electric current. Metals and Materials International, 24(1), 42-50, doi:10.1007/s12540-017-7297-1.

[14] Conrad, H., Karam, N., Mannan, S. and Sprecher, A. (1988). Effect of electric current pulses on the recrystallization kinetics of copper. Scripta metallurgica, 22(2), 235-238.

[15] Conrad, H., Karam, N. and Mannan, S. (1983). Effect of electric current pulses on the recrystallization of copper. Scripta metallurgica, 17(3), 411-416.

[16] Wang, T., Xu, J., Xiao, T., Xie, H., Li, J., Li, T. (2010). Evolution of dendrite morphology of a binary alloy under an applied electric current: An in situ observation. Physical Review E - Statistical, Nonlinear, and Soft Matter Physics, 81(4), doi:10.1103/PhysRevE.81.042601.

[17] Jeong, H. J., Kim, M. J., Park, J. W., Yim, C. D., Kim, J. J., Kwon, O. D. and Han, H. N. (2017). Effect of pulsed electric current on dissolution of Mg 17 Al 12 phases in as-extruded AZ91 magnesium alloy. Materials Science and Engineering A, 684, 668-676, doi:10.1016/j.msea.2016.12.103.

[18] Choi, J., Sung, H. M., Roh, K. B., Hong, S. H., Kim, G. H. and Han, H. N. (2017). Fabrication of sintered tungsten by spark plasma sintering and investigation of thermal stability. International Journal of Refractory Metals and Hard Materials, 69, 164-169, doi:10.1016/j.ijrmhm.2017.08.013. [1] L. Guan, G. Tang, Y. Jiang, P.K. Chu, J. Alloys Compd. 487, 309 (2009).

[19] Y. Estrin, L.S. Tóth, A. Molinari, Y. Bréchet, A dislocation-based model for all hardening stages in large strain deformation. Acta Mater. 46 5509-5522 (1998).

[20] U.F. Kocks, H. Mecking, Physics and phenomenology of strain hardening: the FCC case. Prog. Mater. Sci. 48 171-273 (2003).

[21] A. S. Krausz, K. Krausz, Unified Constitutive Laws of Plastic Deformation (Academic Press, San Diego, 1996)

Chapter 5

Total conclusion

Electrically-assisted manufacturing (EAM) is a promising next-generation process. For commercialization of EAM, understanding on the athermal effect of electric current is necessary. Many theories have been proposed to explain the effect of the electric current. This can be a Joule heating, electromigration, skin effect or pinch effect. Recently, there have been attempts to explain these phenomena with local Joule heating. However, these suggestions are only applicable in certain circumstances. When the electric current is applied to the material, electric charge imbalance occurs around the grain boundary. This charge imbalance promotes atom vibration and lowers the bonding energy. This accelerates the diffusion of atoms around the grain boundary. The concept of effective temperature, which cannot be physically measured, because the atoms behave as if they were at a high temperature is introduced. In order to confirm this effective temperature, electropulsing treatment was applied to the recrystallization of low carbon steel. Two concepts were adopted for the effect of electric current on recrystallization kinetic. One is that the electric current acts like a catalyst to lower the recrystallization activation energy, and the other is the concept of effective temperature as mentioned above.

The recrystallization treatment of low carbon steel was carried out using

electropulsing treatment (EPT), and heat treatment (HT) was performed at the same temperature history as a control group. Through hardness and microstructure analysis, recrystallization occurred at lower temperatures under EPT than under HT. In addition, at the same temperature, it was confirmed that the recrystallization occurred faster under EPT. Arrhenius kinetic analysis confirmed that the recrystallization activation energy was reduced during EPT. This revealed that there is an athermal effect of the electric current.

In the previous study, the experiment had been designed to follow the set temperature in EPT to compare with the HT. At this time, the current density changed to match the intended temperature. This makes it difficult to quantify the athermal effect. Thus, one pulse experiment with the same current density was conducted. It was confirmed that the recrystallization fraction varies depending on the current density. The modified JMAK (Johnson-Mehl-Avrami-Kolmogorov) equation including additivity rule was used for recrystallization kinetic analysis. When predicted only by temperature history, the predicted recrystallization fraction did not correspond to the experimental results. However, when assuming that the recrystallization activation energy was reduced, the calculated recrystallization fraction was in good agreement with the experimental results. In addition, the calculated values were consistent very well with the experimental values, considering that the effective temperature as the athermal effect would accelerate the recrystallization kinetics. The athermal effect increased with the current density. This allowed that the athermal effect, which had been reported only as an

experimental phenomenon was quantified as a function of current density.

In order to apply the previously quantified effective temperature to the electroplasticity, tensile behavior was analyzed by FE constitutive calculation. Trying to calculate the amount of stress drop in pulsed tensile test using only measured temperature history, the calculated value was much lower than the experimental value. When the effective temperature was inserted into the grain boundary, the calculated value was in good agreement with the experimental value. This proved that the athermal effect can be explained by the effective temperature even in electroplasticity.

국문 초록

Electrically-assisted manufacturing (EAM)은 전류를 인가하여 금속의 기계적 특성과 미세구조를 제어하는 공정 기술이다. EAM은 두 가지 연구로 나뉜다. 하나는 변형 도중 펄스 전류를 인가하여 소재의 물성을 제어하는 통전소성이다. 많은 연구자들이 변형 도중 인가된 전류가 항복 응력, 유동 응력 및 연신율과 같은 재료 특성에 영향을 크게 미친다고 보고하였다. 다른 하나는 통전처리로, 변형을 가하지 않는 상태에서 전류를 인가하여 금속 재료의 미세 구조 변화를 제어하는 기술이다. 통전처리는 높은 전류 밀도를 금속 재료에 인가하여 미세구조를 변경하고 물리적 특성을 향상시키는 효과적인 기술이다. 통전 현상의 이해를 통해, 속도론 분석에 기반하여 재결정 거동에 대한 전류의 영향을 평가하였다.

첫번째로, interstitial free (IF) 강에서 재결정 속도에 대한 전류의 영향을 비커스 경도 측정 및 미세구조 관찰을 통해 조사하였다. 냉간 압연 된 소재에 다양한 온도와 시간 조건으로 통전처리와 가열로 열처리를 실시하였다. IF 강의 통전처리 후의 비커스 경도 값은 동일한 열처리 조건에서보다 확연히 낮았다. 미세구조 관찰을 통해 경도 감소는 재결정에 의한 것으로 확인되었다. 이것은 재결정 속도가 저항 발열과는

별개의 전류 자체의 비열 효과에 의해 가속화 되었음을 의미한다. 재결정 속도에 대한 전류의 영향을 구분하기 위해 Johnson-Mehl-Avrami-Kolmogorov (JMAK) 식을 이용하였다. 재결정에서의 핵 생성 속도는 avrami 값에 따라 달라진다고 알려져 있는데, 열처리를 수행했을 때보다 통전처리를 수행했을 때 더 높아 통전처리에서 핵 생성 속도가 더 빠르다는 것을 알 수 있었다. 또한, 아레니우스 식을 통해 통전처리에서 열처리에 비해 재결정 활성화 에너지가 저감 된 것을 알 수 있었다.

두번째로, 1 펄스 실험을 수행하여 전류의 비열 효과에 대한 전류 밀도의 영향을 평가하고자 하였다. 목표하는 피크 온도에 도달하기 위해 전류 밀도 조건에 따라 인가 시간을 다르게 한 단일 펄스 통전처리가 실시되었다. 760, 800℃ 의 피크 온도에서는 전류 밀도가 증가함에 따라 재결정 분율이 감소하다가 특정 전류 밀도 이상으로는 재결정 분율이 증가하는 경향이 있음을 보여준다. 가산 성 규칙을 적용하여 새로 수정된 JMAK 식에 일반적인 가열로 열처리에서 측정된 재결정 분율을 이용하여 파라미터들을 도출하였고, 통전처리에서 얻어진 온도 이력을 이용하여 재결정 분율을 계산하여 실험값과 비교하였다. 계산된 결과와 실험값 비교를 통해 전류의 비열 효과를 구분하였고, 재결정 활성화 에너지 저감 또는 유효 온도 개념의 도입을 통해 전류의 비열 효과를

설명하고자 하였다. 비열 효과를 전류 밀도에 대해 정량적으로 계산하여 전류 밀도가 증가함에 따라 전류의 비열 효과가 증가하는 것을 확인하였다.

마지막으로, 정량화 된 유효 온도를 통전소성에 적용하기 위해, 저탄소강의 인장 거동이 유한요소법 계산에 의해 분석되었다. 고온 인장에 잘 맞는 경화식의 파라미터들을 도출한 이후 통전소성의 온도 이력을 이용하여 통전소성의 인장 거동을 예측하여 실험값과 비교하였다. 앞서 도출된 유효 온도를 적용함으로써 실험에서의 인장 거동과 일치하는 경향을 얻을 수 있었다. 이것은 전류의 비열 효과가 통전소성에서도 유효 온도로 잘 설명될 수 있음을 증명한다.

핵심어: 저탄소강, interstitial free 강, extra deep drawing 급 강, electrically-assisted manufacturing (EAM), 통전소성, 통전처리, 속도론 분석, 비커스 경도, 재결정, 전자후방산란회절 (EBSD), 비열 효과, 유효 온도, 구성식, 유한요소법

Student number: 2014-21447

감사의 글

제가 학위 과정을 소화하는 동안 부족했던 저를 격려해주시고 믿어주신 모든 분들께 감사의 말씀을 드립니다. 힘든 순간마다 여러분들께서 도와주신 덕분에 대학원 생활을 잘 마칠 수 있었습니다.

먼저 지금까지 저를 올바른 길로 인도하고, 항상 제가 가고자 하는 길을 묵묵히 응원해주신 아버지, 어머니께 감사드립니다. 두 분께서 주신 사랑과 믿음은 언제나 제게 큰 힘이 되었습니다. 그리고, 비슷하게 대학원 생활을 하고 먼저 사회에 나가 자기 일을 똑똑하게 잘 해나가고 있는 우원이도 학위 과정 내내 든든한 동반자였고, 항상 고맙게 생각합니다.

부족했던 저를 지도교수님으로서 이끌어주신 한흥남 교수님께 진심으로 감사의 말씀을 드립니다. 교수님께 지도를 받은 6년동안 학문적으로나 인격적으로 더 발전할 수 있었다고 생각합니다. 교수님의 가르침에 따라 앞으로 사회에서 공학박사로서 사회에 기여할 수 있도록 노력하겠습니다. 또한, 교수님께 자주 찾아 뵙고 인사드릴 수 있도록 하겠습니다.

그리고 졸업 논문 심사를 해주신 박은수 교수님, 최인석 교수님, 홍성태 교수님, 김문조 박사님께도 깊이 감사 말씀 드립니다. 심사를 통해 세밀하지 못했던 부분에 대해 다시 한번 상기하고, 새로운 시작을 앞두고 다시 한번 마음을 다잡는 계기가 되었습니다.

긴 시간 동안 함께 지내온 MMMPDL 선후배 분들께도 감사의 말씀 전합니다. 졸업한 이후에도 밖에서 자주 만날 수 있는 인연을 유지했으면 좋겠습니다.

학위 과정 동안 배운 많은 것들과 여러 소중한 인연들 잊지 않겠습니다. 학위 가간 동안 부족한 저와 함께 해 주셨던 모든 분들 다시 한번 감사 드립니다.

2020년 1월 박주원 드림